The important role of stiffnesses values of circular joints on the stress state developed in the tunnel segmental lining

(Article begins on next page)

09 May 2024

ORIGINAL ARTICLE

# The important role of stiffnesses values of circular joints on the stress state developed in the tunnel segmental lining

**Xin Han** · **Pierpaolo Oreste** · **Fei Ye**

**Abstract** Under the application of the fluctuating Tunnel Boring Machine (TBM) jack thrust and the non-uniformly distributed total pressure of the slurry around the lining, the bending and the shear deformation occur on the segmental lining along the longitudinal direction, which cause a stress concentration and increase the damage risk of the segmental tunnel lining. The analysis of the circular joint stiffness is a critical step during the evaluation of the stress state of the segmental lining so as to decrease the associated risk of damage. In order to investigate the lining rings and the circular joint separately, an integrated numerical model which is composed of segment elements and joint elements was developed. Furthermore, stiffness equations for describing in the detail the circular joint behaviour of the tunnel segmental lining are derived. The new stiffness equation of the circular joint is also used to analyse the segment lining behaviour based on a well-known indoor test result by the scientific literature, and satisfactory results were obtained. A simplified estimation of the bending stiffness of the circular joint based on the Boltzmann equation is then suggested in order to obtain quickly its calculation. Finally, based on a specific numerical model, the calculated joint stiffnesses are adopted to analyse the vertical displacement of a real case (The Ningbo metro tunnel in China). Through a developed sensitivity analysis, some useful suggestions are proposed to reduce the damage risk of the segmental lining.

## Article Highlights

- The forces applied by a TBM in the tail to the segmental lining and the buoyancy forces can damage the lining.
- In order to study the stress conditions and the safety factors of the lining it is necessary to evaluate with a certain precision the stiffnesses of the circular joint.
- New equations were developed in order to determine the bending and shear stiffnesses of the circular joints of segmental linings.

X. Han · F. Ye
School of Highway, Chang'an University, Middle-Section of Nan'er Huan Road, Xi'an 710064, Shaanxi, People's Republic of China

X. Han · P. Oreste (✉)
Department of Environment, Land and Infrastructure Engineering (DIATI), Politecnico di Torino, Corso Duca Degli Abruzzi 24, 10129 Turin, Italy
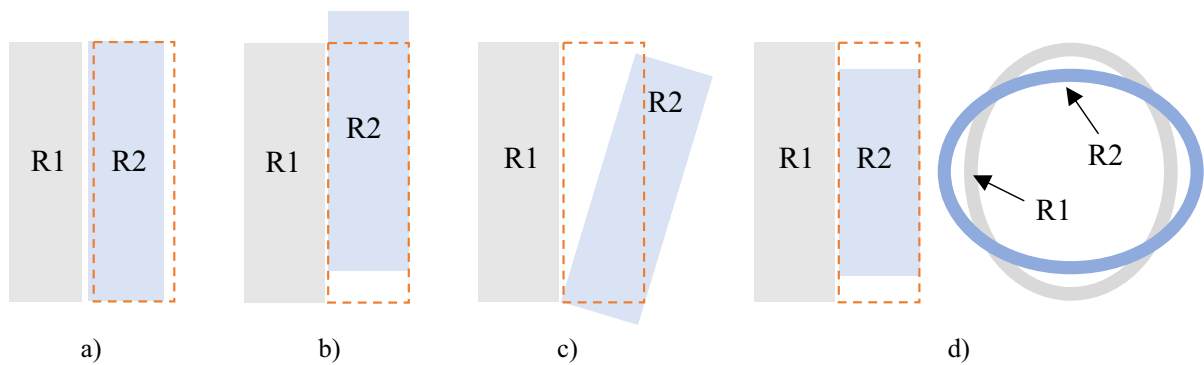e-mail: pierpaolo.oreste@polito.it

**Fig. 1** The types of relative deformation along circumferential joints between adjacent rings. **a** compression; **b** dislocation; **c** rotation; **d** transversal deformation. Key: R1 means the lining ring 1, and R2 means the ring 2

# 1 Introduction

The method of dividing the tunnel lining into segments is widely adopted in tunnel engineering with Tunnel Boring Machines (TBMs); segmental lining is favourable for centralized and factory production, convenient transportation, and efficient installation. Generally, segmental linings are made from concrete and steel, and are connected by bolts along the longitudinal and transverse directions. Different from the integral pouring concrete lining, the structure discontinuity due to the circumferential and longitudinal joints is the main physical characteristic of a segmental lining and significant relative dislocations and openings can be verified in each joint.

The segmental rings are the basic element along the tunnel axis. The relative deformation between the adjacent rings along the circumferential joint can be divided into four types: compression, dislocation, rotation and transversal deformation (Fig. 1); they are caused by the normal force, shear force, bending moment and lateral (radial) pressure. The compression, dislocation and rotation deformation of the segmental lining ignores a relative deformation among the segments of the lining rings (Fig. 1d).

Based on a full-scale test of the single segmental ring, Liu et al. (2015) confirmed that the main reason which leads to the failure of a single segmental ring is the longitudinal joint damage, and the longitudinal joints are the weakest location and the earliest yield point. Furthermore, Liu et al. (2020b) tested the influence of the adjacent segmental rings with a staggered assembly which means the longitudinal joint is not on the same straight line in all the rings, and

found that the distribution of the moment was influenced by the adjacent segmental rings which led to a moment increase in the segment body and a moment decrease in the longitudinal joints; therefore the failure of segmental linings begins at the circumferential joints due to the compressive-shearing failure of tongue-groove tenon. Ye et al. (2014) investigated the straight assembly and the staggered assembly by an indoor model test and explained the effect of the location of a longitudinal joint of the adjacent rings on the rings' deformation in the transversal section. These researches reveal that the circumferential joints can redistribute the ring's deformation, and make the segmental lining more uniform (Fig. 1d).

The uniform longitudinal compression deformation is the ideal deformation of the circumferential joint, which cannot lead to the concentration of longitudinal stresses (Fig. 1a). However, since the circumferential surface of adjacent rings has a lower stiffness compared with the segmental rings, a dislocation and a rotation between the surface of the adjacent rings can develop (Fig. 1b, c). The rotation deformation will cause an uneven distribution of longitudinal stresses on the transversal section of the circular joint, which leads to the increase of the damage risk to the joint (Gil Lorenzo 2019). The dislocation deformation usually generates shear stresses on the segmental lining (Liu et al. 2021), especially for the joints with the tongue and groove tenon.

The accumulation of the dislocation and rotation along the tunnel axis will lead to differential deformation due to the lining buoyancy or subsidence phenomenon along the longitudinal direction of the tunnel. The differential deformation is therefore the

critical index to assess the quality of a tunnel because it will lead to a higher damage risk of the concrete breakage in the segmental lining (Han et al. 2018).

Chen et al. (2016) reported the monitoring results of the Ningbo Metro Line 1 (China), which led to differential displacements, cracks and leakages in the tunnel lining. Huang et al. (2020) reported a soil–water rush causing differential displacements and the lining damage in Tianjin Metro Line 1 (China), and observed that the maximum value of the ground surface settlement, the tunnel crown displacement and the lateral convergence were about 119 mm, 3.8 mm and 22 mm respectively. Liu et al. (2020a) discussed about an accident occurred in a leakage location inside a tunnel during freezing construction, which lead to the uneven settlement and the concrete spalling along the circumferential joints. These cases describe that the obvious change of lateral force applied on the segmental lining leads to differential displacements which result in the dislocation and rotation between the lining rings and further causes the damage of lining joints.

Differential displacements are also very common during the construction phase (Chen et al. 2018; Zhou and Ji 2014). A 120 mm maximum ultimate uplift value was verified by Zhou and Ji (2014) in the construction period of a 6.2 m external diameter tunnel. Different reasons can be considered: jacks thrust, grouting pressure and surrounding rock conditions. Zhou and Ji (2014) revealed that the composition of slurry and grouting pressure have a significant influence on the vertical displacement, while jacks thrust, advance rate of the TBM and the pressure of the shield chamber have a little impact.

Nowadays, there are two types of slurry as synchronous grouting material: single-component slurry and two-component slurry. Compared with the two-component slurry which is composed of cement, fly ash, bentonite, etc. (A) and sodium silicate (B), and is grouted by a special grouting equipment, the single-component slurry is composed of cement, bentonite, sand, etc., and has a lower risk of blockage of the grouting pipe with a lower requirements for grouting equipment. The disadvantage of the single-component slurry is the long setting time which increase the uplift risk (Peila et al. 2011) due to the lining buoyancy in the fluid slurry zone.

In order to quickly and simply assess the differential deformations of the tunnel lining along the longitudinal direction, 1D simplified analytical models were developed based on the beam theory which adopt the bending stiffness and the shear stiffness to control the longitudinal deformation (Cheng et al. 2021; Li et al. 2019; Liang et al. 2017; Liao et al. 2008; Liu et al. 2021; Shi et al. 2022; Shiba et al. 1989; Wu et al. 2015; Yu et al. 2019). Because the stiffness is an equivalent value that is influenced by the material of the segmental lining, the shape of its cross section and the presence of forces, especially for the joints, the evaluation method of the stiffness is controversial and also in continuous improvement (Cheng et al. 2021; Wu et al. 2015). Li et al. (2019) emphasized that the longitudinal axial forces have a significant influence for the longitudinal bending stiffness through an indoor test, and they need to be considered during the evaluation of the bending stiffness of the segmental lining. Geng et al. (2019) divided the deformation of the circumferential joint into five different patterns based on the contact state of the joint and the stress state of bolts, and found that the combination of tension force and moment influence the equivalent bending stiffness. Shi et al. (2022) considered a nonlinear equivalent bending stiffness of joints under the application of axial forces, and found that the deformation of joints shows a two-stage increase with the increase of the moment. Based on the findings of researchers, the axial force in the lining has an obvious impact on the bending stiffness, and the relationship between them is nonlinear and not explicit.

The joints are the weakest parts in the segmental lining, and their stiffness, which is used to represent the relationship between the load and the deformation, is influenced by numerous factors; after the joint opening (Li et al. 2019) it is possible to see a decrease in the stiffness value. Moreover, taking a detailed assessment of the joint stiffness and its influence on the stress state of the segmental lining with the application of a normal force and a moment is important for analysing the damage risk of segmental linings.

In this paper, considering the deformation of the joint with a specific length and the deformation of the segmental lining ring separately, the bending stiffness of the circular joint is derived based on the concrete compressed stiffness and the steel tensile stiffness which is converted to an equivalent one. 36 analysed cases with different tunnel external diameters, thicknesses of the segmental lining and bolting systems
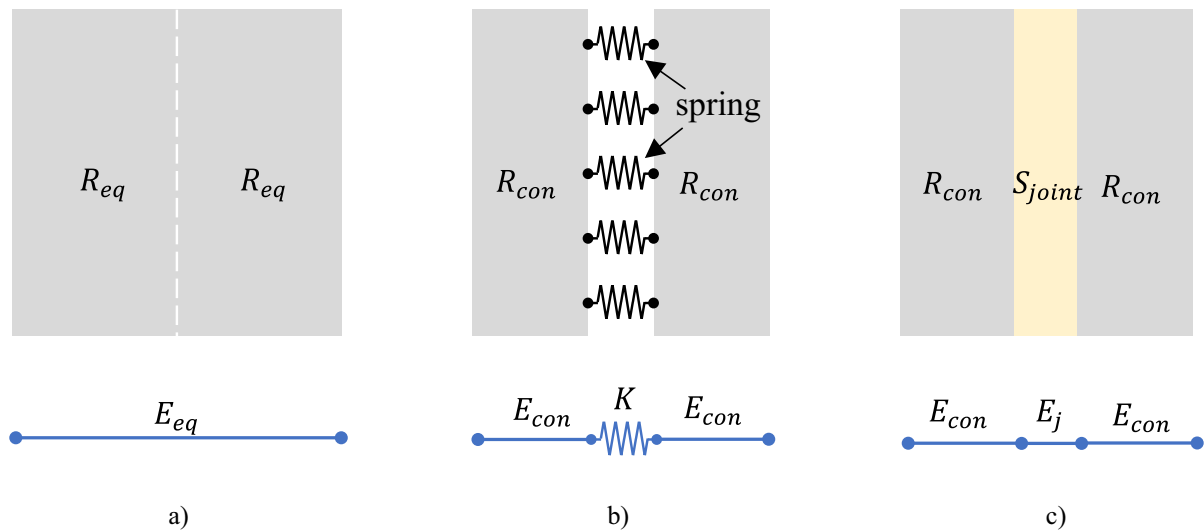
**Fig. 2** Simplified analytical models of circumferential joint: **a** continuous beam model; **b** beam-spring model; **c** standard and special beam model. Key: $R_{eq}$ means equivalent ring, $R_{con}$ means standard ring, and $S_{joint}$ means the special ring for the joint simulation

are studied; a simplified equation for the joint bending stiffness is proposed. The joint bending stiffness is no longer a constant, and is a function of the normal force and of the moment applied to the circular joint.

Based on the bolt deformation and the constraint of the bolt hole, a procedure used to calculate the equivalent shear stiffness of the circular joint is also proposed. The influence of the bolt combination and the gap between the bolt and the hole on the shear stiffness are analysed. This model allows to evaluate the contribution of the concrete hole wall and not only of the bolt to the shear stiffness. The obtained results of the study were able to give some suggestions to reduce the damage risk of the segmental lining during the construction of a tunnel using a TBM machine.

## 2 The circular joint behaviour of a segmental lining

### 2.1 Short review of solutions for stiffnesses determination in the scientific literature

The analytical method and the empirical one are two main ways to design the tunnel lining (Einstein and

Schwartz 1979). The finite element analysis (one type of the numerical method) is sophisticated and time-consuming, but is widely used due to its capability of detailed simulation for the segmental lining, such as bolts, concrete segments, hydraulic jacks, jack pad, shield tail wire brush, etc. (Chaipanna and Jongpradist 2019; Gil Lorenzo 2021; Guo et al. 2021; Shi et al. 2022; Wang et al. 2014; Zaheri et al. 2020). Simplified analytical methods are also widely applied for the fast evaluation of tunnel lining based on the geotechnical and geometrical information (Einstein and Schwartz 1979); it simplifies the tunnel lining as beams or beams connected by springs (Chen et al. 2018; Cheng et al. 2021; Geng et al. 2019; Gil Lorenzo 2019; Huang et al. 2015, 2012; Li et al. 2019; Liang 2019; Liang et al. 2021, 2017; Liu et al. 2021; Wu et al. 2015; Yu et al. 2019).

Based on the scientific literature, there are about three types of the simplified analytical models used to analyse the deformation of the segmental lining along the longitudinal direction, including the continuous beam model (CB), beam-spring model (BS) and the standard and special beam model (SSB) (Fig. 2). The longitudinal segmental lining is seen as a homogeneous beam in the CB model which was derived by Shiba et al. (1988) (Fig. 2a). Huang et al. (2012), Talmon and Bezuijen (2013), Huang et al. (2015) and Gil Lorenzo (2019) developed

the longitudinal continuous model based on the Euler–Bernoulli beam and analysed the longitudinal deformation and the internal forces. However, the Euler–Bernoulli beam can't represent the shear deformation; the continuous Timoshenko beam was used to calculate the longitudinal deformation considering the bending stiffness and the shear stiffness (Cheng et al. 2021; Shi et al. 2022; Wu et al. 2015, 2018). Although the CB model was used widely as a result of the convenience, it is difficult to accurately reflect the deformation characteristic of joints after considering the discontinuous segmental lining as an equivalent continuous beam (Li et al. 2014). The BS model which is proposed by Koizumi et al. (1988) simulates the segmental lining and joints with beams and springs (Fig. 2b), and can make up for the deficiencies of the CB model. However, the spring stiffness of the circular joint is complicated to determine.

To analyse the sinking of a Micro Tunnel Boring Machine (MTBM) in soil, Oreste et al. (2002) considered that the tunnel was composed of the MTBM, the pipes and the joints, and adopted the hyperstatic reaction method to calculate the longitudinal deformation; it was developed based on the finite difference method.

In this paper, the joint is considered as a special beam, and segments are simulated by standard beam (Fig. 2c). The stiffness of segments are relatively simple to evaluate (Cheng et al. 2021), while stiffnesses of the joint elements, including both the bending stiffness and the shear stiffness, are difficult and are discussed in this section based on the application of the moment, the normal force and the shear force at each joint. The proposed approach aims to determine the characteristics of the special elements that are able to simulate circular joints in the longitudinal modelling of the segmental lining.

## 2.2 Rotational effect and opening of the joint due to moments and normal forces

Based on the Timoshenko beam theory, the ratio between the moment $M$ and the relative rotation angle $\omega$ of the cross sections for a length $L$, can be calculated based on the bending stiffness $EI$ and $L$.

$$\frac{M}{\omega} = \frac{EI}{L} \tag{1}$$

where $EI$ is the bending stiffness of the beam with a length $L$; it is an equivalent bending stiffness for a beam simulating a joint: $EI = (EI)_{eq}$.

Therefore, the bending stiffness is the critical parameter for the evaluation of the bending deformation of the beam under transversal loads (Eq. 1). However, due to the opening of the joint under moments and normal forces, the relationship between the rotation angle and the moment is nonlinear.

In order to obtain this relationship, the stress state of bolts and of concrete at the circumferential joint is analysed with the application of a moment and a normal force (Fig. 3). There are two types of conditions: joint closed and joint open (Fig. 4). When the joint is closed, the whole cross section is compressed and the neutral axis is out of the cross section (Fig. 4a). When the joint is open, the cross section is divided into a detached zone and a compressed one (Fig. 4b).

When the joint is closed, the total cross section of the segmental lining is compressed (Fig. 4a). The rotation angle $\theta$ can be obtained based on the developed longitudinal displacements.

$$\theta = \frac{2 \cdot (\delta_{c,max} - \delta_{c,min})}{2 \cdot R_e} \tag{2}$$

The compression displacement of the concrete ($\delta_c$) is equal to the ratio between the stress and the compression stiffness of the concrete based on the Winkler theory.

$$\delta_c = \frac{\sigma_c}{K_c} \tag{3}$$

where $K_c$ is the compression stiffness of the concrete, $\sigma_c$ is the compression stress of concrete.

Furthermore, the difference between the maximum compression stress $\sigma_{c,max}$ and the minimum stress $\sigma_{c,min}$ can be determined by the following equation based on the beam theory:

$$(\sigma_{c,max} - \sigma_{c,min}) = \frac{2 \cdot M \cdot R_e}{I} \tag{4}$$

where $M$ is the moment, $\sigma_{c,max}$ and $\sigma_{c,min}$ are the maximum and minimum compression stress of the concrete, $I$ is the inertia moment of the segmental lining ring.

Substituting Eqs. 2 and 3 into Eq. 4, the following equation represent the bending deformation of the joint.
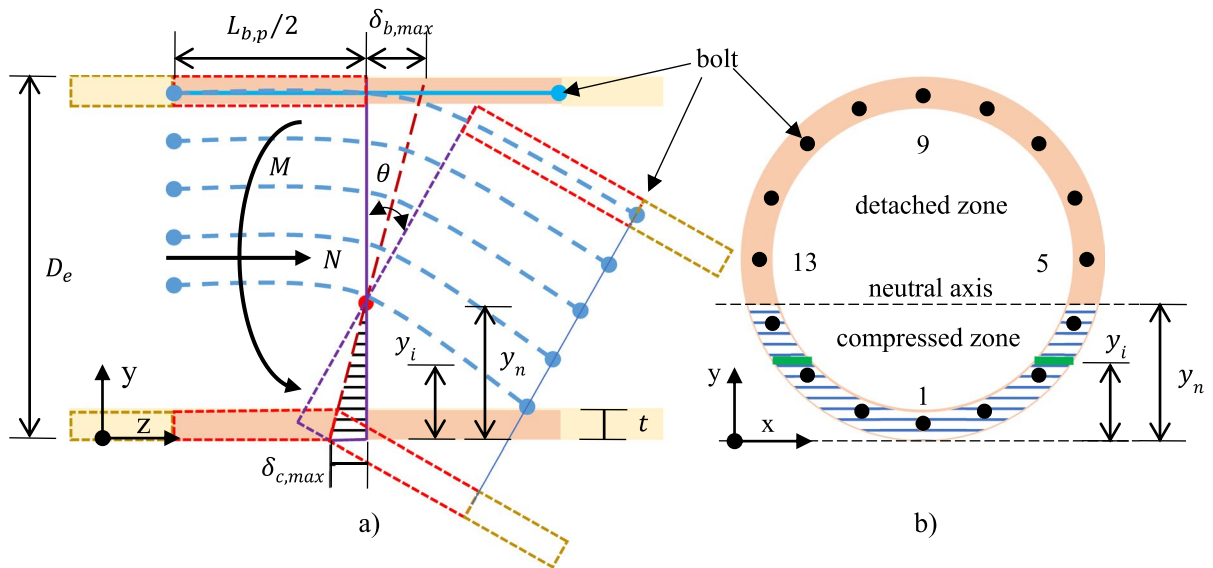
**Fig. 3** The tensional and deformative condition of a circular joint when a moment $M$ and a normal force $N$ are applied (case of 16 bolts connecting the circular joint). Key: **a** longitudinal view; **b** transversal view. Legend: $D_e$ is the external diameter of the tunnel, $t$ is the thickness of the segmental lining, $L_{b,p}$ is the projection length of the bolt along the axial direction, $\delta_{b,max}$ is the maximum tensile displacement of the bolts on the joint cross section, $\delta_{c,max}$ is the maximum compression displacement of the concrete, $\theta$ is the rotation angle of the joint which is the relative rotation angle of the end surface of segment with the adjacent one, $y_i$ is the location of the assumed strips in the integral method, $y_n$ is the location of the upper boundary of the compressed zone of the section
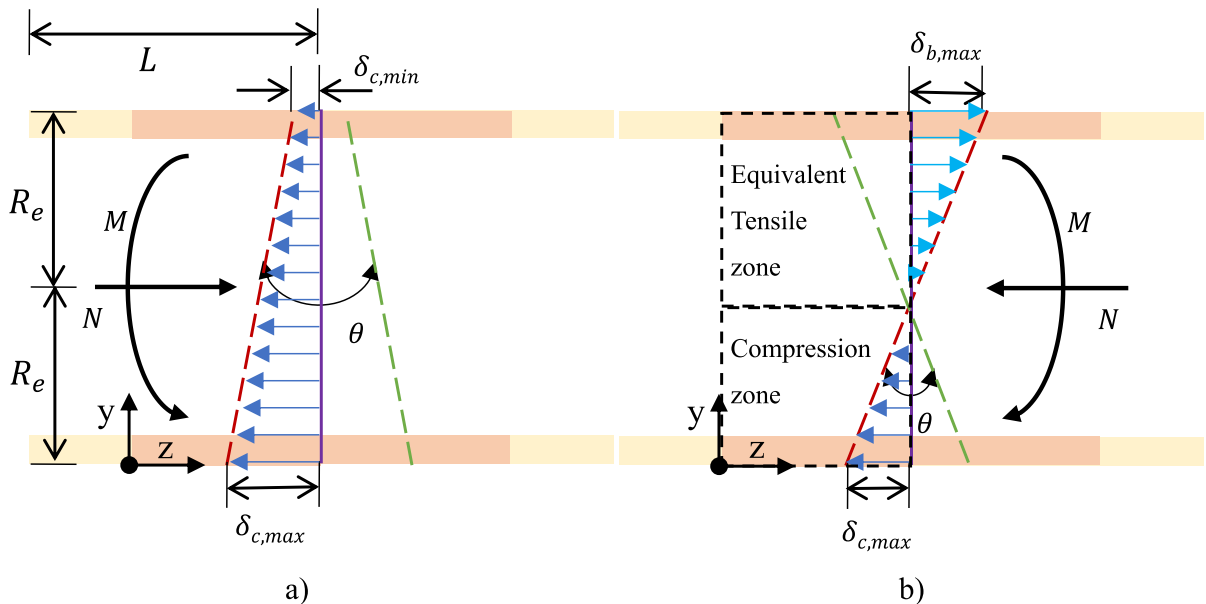


**Fig. 4** Developed displacements on the circular joint. Key: **a** joint closed; **b** joint open. (Assumption: the contact surface still keeps a plane section after rotational deformation). Legend: $R_e$ is the external radius of the tunnel, $\delta_{c,min}$ is the minimum compression displacement of the concrete in the cross section, $L$ is the length of segmental lining near the joint along the axial direction which influences the compressed displacement $\delta_c$ of the concrete (Eqs. 7 and 8)

$$\frac{M}{\omega} = \frac{I \cdot K_c}{2} \tag{5}$$

For the condition of the joint closed, the bending stiffness is equal to the bending stiffness of the segmental lining (Eq. 1):

$$(EI)_{eq} = E_{con}I \tag{6}$$

where $E_{con}$ is the elastic modulus of concrete.

Therefore, the compression stiffness of concrete can be derived using the following equation.

$$K_c = \frac{2 \cdot E_{con}}{L} \tag{7}$$

Based on Eq. 1, the rotation angle of the beam with a bending stiffness $EI$ under the application of the moment $M$ is a relative value which is influenced by the length $L$. Because the compression displacement of the concrete $\delta_c$ is a process variable and the stress of the concrete is a state variable (Eq. 3), the compression stiffness is also a process variable and can change with the length $L$.

On the other hand, the rotation of the joint when the joint is open in the detached zone is determined by the deformation of the bolts with a length $L_b$; the corresponding length $L_{b,p}$ of the segment lining which wraps the bolts and provided the bolts holes does not have any deformation (Fig. 3a). Assuming that the contacted surface of the joint still keeps a plane section after bending deformation, the following equation can present the compression deformation on the compression zone of the joint element with a length $L_{b,p}$.

$$K_c = \frac{2 \cdot E_{con}}{L_{b,p}} \tag{8}$$

When the joint is open, there is a detached zone and a compressed zone (Fig. 3). The strain of the bolt is equal to the ratio between the tensile stress and the elastic modulus of the bolt, and also the ratio between the displacement and length of the bolt.

$$\varepsilon_b = \frac{2 \cdot \delta_b}{L_b} = \frac{\sigma_b}{E_{st}} \tag{9}$$

where $\sigma_b$ is the tensile stress in the bolt, $E_{st}$ is the steel elastic modulus, and $\delta_b$ is the elongation of the bolt

due to the joint opening and can be obtained by the tensile stress $\sigma_b$ and the tensile stiffness of the bolt $K_b$.

$$\delta_b = \frac{\sigma_b}{K_b} \tag{10}$$

Therefore, the tensile stiffness of the bolt can be derived by the following equation:

$$K_b = \frac{2 \cdot E_{st}}{L_b} \tag{11}$$

Based on the transformed area method, the bolt stress can be commuted into an equivalent tensile stress in its competence area of the cross section of the segmental lining.

$$\sigma_{bs} \cdot \frac{A}{n} = \sigma_b \cdot A_b \tag{12}$$

where $n$ is the number of the bolts, $A_b$ is the cross-section area of the bolt, $A$ is the one of the lining ring, $\sigma_{bs}$ is the equivalent tensile stress where the joint is open. Where the equivalent tensile zone take place the same displacement as the bolts, but the tensile stiffness and the stress of this zone is different from the bolts.

The equivalent tensile stress is equal to the tensile stiffness of the equivalent area $K_{bs}$ multiplied by the bolt elongation,

$$\sigma_{bs} = K_{bs} \cdot \delta_b \tag{13}$$

where

$$K_{bs} = K_b \cdot \frac{n \cdot A_b}{A} \tag{14}$$

The joint can be simplified as a Bimodular beam with a length $L_{b,p}$ which is composed of the equivalent tensile zone and the compressed zone after the joint opening (Fig. 4b). The tensile stiffness and the compression stiffness for the two zones can be calculated by the following equation.

$$\begin{cases} K_{com} = K_c = \frac{2 \cdot E_{con}}{L_{b,p}} & 0 \leq y \leq y_n \\ K_{ten} = K_{bs} = \frac{2 \cdot E_{st}}{L_b} \cdot \frac{n \cdot A_b}{A} & y > y_n \end{cases} \tag{15}$$

**Fig. 5** The distribution of the deformation and the stress state along the circular joint cross section. Key: **a** is the cross section of a joint, **b** is the deformation of the joint varying the height y, and **c** is the stress state of the joint varying the height y



a)

b)

c)
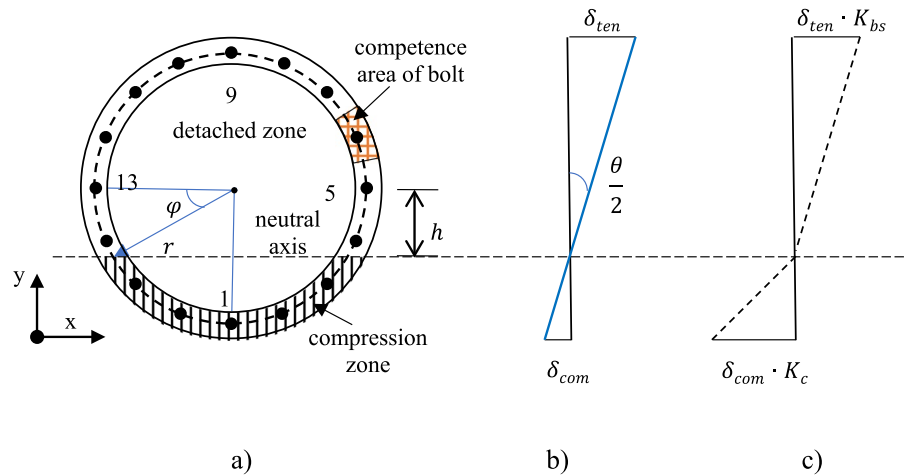
where $y_n$ is the vertical height of the compression zone (Fig. 3).

## 2.3 Bending stiffness of the joint

Based on the Bimodular beam simulating the joint (Fig. 5), the stress state can be obtained by the stiffness and deformation of the joint as follows:

$$\begin{cases} \sigma_{com} = K_{com} \cdot \delta_{com} \\ \sigma_{ten} = K_{ten} \cdot \delta_{ten} \end{cases} \quad (16)$$

The normal force N and the moment M of the joint can be connected to the stress value in the joint by the following equations:

$$\begin{cases} N = \int_A \sigma \cdot dA \\ M = \int_A \sigma \cdot (R_e - y) \cdot dA \end{cases} \quad (17)$$

They can also be expressed as follows:

$$\begin{cases} N = \frac{\theta}{2} \cdot \int_0^{2R_e} K \cdot b(y) \cdot (y_n - y) \cdot dy \\ M = \frac{\theta}{2} \cdot \int_0^{2R_e} K \cdot b(y) \cdot (y_n - y) \cdot (R_e - y) \cdot dy \end{cases} \quad (18)$$

where $K$ is the stiffness which can be obtained by Eq. 15, $b(y)$ is the total width of the cross section varying the height y.

Based on Eq. 1, the equivalent bending stiffness of the joint can be obtained by the following equation:

$$(EI)_{eq} = \frac{M}{\theta} \cdot L = \frac{L_{b,p}}{2} \cdot \int_0^{2R_e} K \cdot b(y) \cdot (y_n - y) \cdot (R_e - y) \cdot dy \quad (19)$$

The angle $\varphi$ was used to describe the location of the neutral axis by Shiba et al. (1988) (Fig. 5). The displacement of the compression and the tensile zones can be connected to the angle $\theta$:

$$\begin{cases} \delta_{com} = (r - h) \cdot \frac{\theta}{2} \\ \delta_{ten} = (r + h) \cdot \frac{\theta}{2} \end{cases} \quad (20)$$

where $r$ is the average radius of the segmental lining

$$r = R_e - \frac{t}{2} \quad (21)$$

$t$ is the thickness of the segmental lining.

$h$ is the vertical distance from the central point to the highest point of the compression zone:

$$h = r \cdot \sin\varphi \quad (22)$$

Based on Eq. 18, the moments referred to the horizontal axis passing through the central point of the lining cross-section can be derived on the two zones when the joint is open:

$$\begin{cases} M_{com} = \frac{2 \cdot K_{com} \cdot \delta_{com}}{r - h} \cdot \int_0^{\frac{\pi}{2} - \varphi} (r \cdot \cos\alpha - h) \cdot r^2 \cdot \cos\alpha \cdot t \cdot d\alpha \\ M_{ten} = \frac{2 \cdot K_{ten} \cdot \delta_{ten}}{r + h} \cdot \int_0^{\frac{\pi}{2} + \varphi} (r \cdot \cos\alpha + h) \cdot r^2 \cdot \cos\alpha \cdot t \cdot d\alpha \end{cases} \quad (23)$$

where $M_{com}$ is the moment obtained by the stresses in the compression zone and $M_{ten}$ is the moment obtained by the stresses in the detached zone.

The total moment of the joint is the sum of the moments of the two zones:

$$M = \left[ K_{com} \cdot \left( \frac{\pi}{2} - \varphi - \sin\varphi \cdot \cos\varphi \right) \right.$$
$$\left. + K_{ten} \cdot \left( \frac{\pi}{2} + \varphi + \sin\varphi \cdot \cos\varphi \right) \right] \cdot \frac{(D_e - t)^3 \cdot t}{16} \cdot \theta \tag{24}$$

According to Eq. 1, the equivalent bending stiffness of the joint element with a length $L_{b,p}$ can be derived:

$$(EI)_{eq} = \left[ K_{com} \cdot \left( \frac{\pi}{2} - \varphi - \sin\varphi \cdot \cos\varphi \right) \right.$$
$$\left. + K_{ten} \cdot \left( \frac{\pi}{2} + \varphi + \sin\varphi \cdot \cos\varphi \right) \right] \cdot$$
$$\frac{(D_e - t)^3 \cdot t}{16} \cdot L_{b,p} \tag{25}$$

Based on Eq. 18, the normal force on the two zones can be obtained by the following equations:

$$\begin{cases} N_{com} = \frac{2 \cdot K_{com} \cdot \delta_{com}}{r - h} \cdot \int_0^{\frac{\pi}{2} - \varphi} (r \cdot \cos\alpha - h) \cdot r \cdot t \cdot d\alpha \\ N_{ten} = \frac{2 \cdot K_{ten} \cdot \delta_{ten}}{r + h} \cdot \int_0^{\frac{\pi}{2} + \varphi} (r \cdot \cos\alpha + h) \cdot r \cdot t \cdot d\alpha \end{cases} \tag{26}$$

where $N_{com}$ is the compression normal force and the $N_{ten}$ is tensile normal force.

When the total normal force of the contact surface of the joint is equal to zero, $N_{com} = N_{ten}$, the angle $\varphi$ can be derived by the following equation:

$$\varphi + cot\varphi = \pi \cdot \left( \frac{1}{2} + \frac{K_{ten}}{K_{com} - K_{ten}} \right) \tag{27}$$

When the total normal force is not equal to zero (it means that the compression force is larger than zero during the construction stage), the normal force N is obtained as:

$$N = \left[ K_{com} \cdot \left( \cos\varphi - \sin\varphi \cdot \left( \frac{\pi}{2} - \varphi \right) \right) \right.$$
$$\left. - K_{ten} \cdot \left( \cos\varphi + \sin\varphi \cdot \left( \frac{\pi}{2} + \varphi \right) \right) \right] \cdot$$
$$\frac{(D_e - t)^2 \cdot t}{4} \cdot \theta \tag{28}$$

Dividing the total normal force by the moment, the following equation which is used to calculate the angle $\varphi$ can be derived from Eqs. 24 and 28. In order to simplified the equation, the parameters $m$ is introduced:

$$\frac{N}{M} \cdot \frac{D_e - t}{4} = \frac{m \cdot (\cos\varphi + \varphi \cdot \sin\varphi) - \pi/2 \cdot \sin\varphi}{-m \cdot (\varphi + \cos\varphi \cdot \sin\varphi) + \pi/2} \tag{29}$$

where

$$m = \frac{K_{com} - K_{ten}}{K_{com} + K_{ten}} \tag{30}$$

In this section, two methods able to calculate the bending stiffness of a circular joint, have been presented:

(1) the integral method: based on Eqs. 18 and 19, dividing the joint section into many strips with a short height $\Delta y$; then, the normal forces and the moments can be obtained by summing along the vertical direction y.

(2) The angle $\varphi$ simplified method: the joint bending stiffness can be obtained by Eq. 25. In this equation, the angle $\varphi$ can be calculated by using Eq. 27 when the normal force is equal to 0 and by Eq. 29 when the normal force is greater than 0.

Compared with the second method, the first one can consider also the yielding of steel bolts and concrete. Although the second method is only available for elastic materials, it provides a possibility to quickly calculate the bending stiffness of a circular joint. A more simplified method is suggested on Sect. 3 based on the second method, and the limitation moment of a joint under the application of the normal force N is discussed.

## 2.4 Dislocation effect of the lining rings due to the shear force

Based on the Timoshenko beam theory, shear stiffness is a critical parameter for the evaluation of the shear deformation of beams. Based on shear deformation tests (Liu et al. 2018; Yan et al. 2011), the shear deformation of a circumferential joint can be divided into three stages (Cheng et al. 2021): (a) no shear deformation under the friction forces on the joint faces; (b) free shear deformation due to the gap between the hole walls and the steel bolts; (c) restricted shear deformation based on the resistance of the bolt or the tongue and groove tenon. The test results show that the first and the second stages may occur simultaneously due to the mistake of assembly (Liu et al. 2018).

**Fig. 6** The shear deformation of the connecting bolt in its hole. Key: **a** initial state; **b** limit state of the free shear deformation before the contact with the hole wall; **c** restricted shear deformation
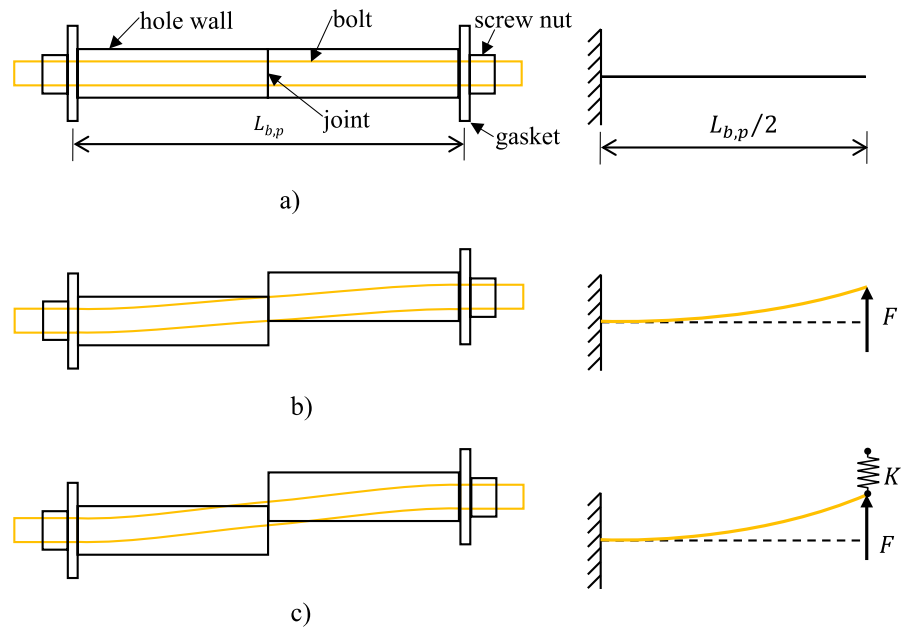


Because the shear deformation mainly occur in the joint due to the dislocation between the adjacent rings (Wu et al. 2015), the equivalent shear stiffness of a circular joint can be obtained by the following equation:

$$(kGA)_{j,eq} = \frac{Q_{max}}{\delta_{j,max}} \cdot L_{b,p} \tag{31}$$

where $(kGA)_{j,eq}$ is the equivalent shear stiffness, $Q_{max}$ is the maximum shear force of the joint, $\delta_{j,max}$ is the maximum dislocation of two adjacent rings, $L_{b,p}$ is the projection length of the bolts along the longitudinal direction, and is also the length of the element that simulates the joint (Fig. 6). Figure 6 shows a simplified scheme where the bolt length is represented by the projection along the lining axis.

When the stress in the bolts reaches the limit yield stress $\sigma_y$, the developed maximum shear force of each bolt in the joint can be obtained; then the maximum shear force of the joint $Q_{max}$ is obtained by the following equation:

$$Q_{max} = \frac{\sqrt{3} \cdot n}{16} \cdot \pi \cdot \phi_{bolt}^2 \cdot \sigma_y \tag{32}$$

Before the shear deformation of the bolt, the bolt is located in the centre of the bolt hole (Fig. 6a). Due to the gap between the diameter of the hole and of the bolt, the bolt will bend with the shear deformation of the segmental lining. The bolt bending deformation is without the restriction of the hole wall before reaching the limit condition when the bolt is in contact with the hole wall (Fig. 6b). After this limit state, the deformation of the bolt will be restricted by the hole wall (Fig. 6c). Therefore, based on the described limit state, the shear deformation of the bolt can be divided into two zones: free shear deformation and restricted shear deformation.

Due to the constraint of the screw nut, the end-point of the bolt is considered to be a fixed end, and the cantilever beam can be used to simulate the bending deformation of the bolt under the application of the shear force (Fig. 6a): the displacement of the bolt relative to the hole wall has the maximum value in the middle of the bolt length (Fig. 6b). When the bolt touches the hole wall, the resistance from the hole wall is applied on the bolt together with the force from the other half of the bolt (Fig. 6c). The resistance from the hole wall can be calculated by the compression stiffness of the concrete hole wall.

The relative shear displacement of the segmental lining $\delta_j$ is two times the transversal displacement of the bolt in the middle of the bolt length $\omega(L_b/2)$.

$$\delta_j = 2 \cdot \omega(L_b/2) \tag{33}$$

For the free shear deformation, the displacement of the bolt can be obtained based on the bending deformation of the cantilever beam.

$$\omega(L_b/2) = \frac{Q}{n} \cdot \frac{(L_b/2)^3}{3 \cdot E_{st} \cdot I_{bolt}} \tag{34}$$

where $Q$ is the shear force of the joint, $I_{bolt}$ is inertia moment of the bolt cross-section, $E_{st}$ is the steel elastic modulus.

When the shear deformation reaches the limit state, the transversal displacement is equal to half of the difference between the diameter of the hole and the diameter of the bolt. The limit shear force $F_{lim}$ can be derived by the following equation:

$$F_{lim} = \frac{12 \cdot (\phi_{hole} - \phi_{bolt}) \cdot E_{st} \cdot I_{bolt}}{L_b{}^3} \tag{35}$$

For the restricted condition, the transversal displacement of the bolt can be obtained based on the cantilever beam theory:

$$\omega(L_b/2) = \left( \frac{Q}{n} + K_{hole} \cdot \frac{\phi_{hole} - \phi_{bolt}}{2} \right) \cdot \frac{L_b{}^3}{K_{hole} \cdot L_b{}^3 + 24 \cdot E_{st} \cdot I_{bolt}} \tag{36}$$

where $K_{hole}$ is the compression stiffness of the hole wall, $K_{hole}$ can be estimated by the following equation (Han et al. 2022):

$$K_{hole} = \frac{4}{\sqrt{\pi}} \cdot \frac{G_{con}}{(1 - v_{con})} \cdot \sqrt{A_c} \tag{37}$$

The area $A_c$ of the concrete compressed zone is equal to the diameter of the bolt $\phi_{bolt}$ multiplied by the length of the compressive zone $L_c$: $A_c = \phi_{bolt} \cdot L_c$. $L_c$ can be obtained by the displacement $\omega(L_b/2)$ and the first derivative of displacement $\omega'(L_b/2)$:

$$L_c = \frac{1}{\omega'(L_b/2)} \cdot \left[ \omega(L_b/2) - \frac{\phi_{hole} - \phi_{bolt}}{2} \right] \tag{38}$$

where the first derivative of displacement $\omega'(L_b/2)$ is:

$$\omega'(L_b/2) = \left[ \frac{Q}{n} - K_{hole} \cdot \left( \omega(L_b/2) - \frac{\phi_{hole} - \phi_{bolt}}{2} \right) \right] \cdot \frac{(L_b/2)^2}{2 \cdot E_{st} \cdot I_{bolt}} \tag{39}$$

Based on Eqs. 36–39, the displacement $\omega(L_b/2)$ can be calculated under the application of the shear force $Q$ through an iterative procedure varying $K_{hole}$, starting from an initial value of $K_{hole} = 0$ and finishing after achieving a certain accuracy in the final result.

Therefore, according to the comparison between the maximum shear force developed inside each bolt $Q_{max}/n$ and the limit shear force $F_{lim}$, the contact between the bolt and the hole wall can be evaluated. Furthermore, the maximum dislocation of the joint $\delta_{j,max}$ can be calculated by the Eqs. 33 and 34 or from Eqs. 36 to 39 under the application of the maximum shear force $Q_{max}$. The detailed procedure for the calculation of the equivalent shear stiffness is shown in Fig. 7.

## 3 Cases study for evaluating the circumferential joint behaviour

### 3.1 Bending stiffnesses of the circumferential joint

The integral method of Sect. 2.3 has been applied to the case of the Metro Tunnel of Ningbo in China; the lining rings have a width of 1.2 m, a thickness of 0.35 m, an external diameter of 6.2 m, and a bolt system of 16 longitudinal bolts with a diameter of 30 mm (cross section area of 561mm$^2$), a length of 530 mm, and a projection length of 400 mm. The main material of the lining segments is a C50 concrete; the Young's Modulus, the Poisson's ratio and the unit weight of concrete are $3.45 \times 10^4$ MPa, 0.167 and 25 kN/m$^3$ respectively. In addition, the bolt material is a 8.8 class steel; the Young's Modulus and the Poisson's ratio are $2.06 \times 10^5$ MPa, 0.3 respectively (Zhou and Ji 2014).

In order to investigate the influence of the main lining parameters on the stiffnesses of the circumferential joint, a further 36 different cases were also considered with different tunnel diameters, thicknesses of the segmental lining, bolt diameters and applied

**Fig. 7** Procedure for the calculation of the equivalent shear stiffness $((kGA)_{j,eq})$. Key: $K_m$ is the initial value of the compression stiffness of the hole wall $K_{hole}$ and is used to calculate the parameters before getting the next value $K_n$ by Eq. 37
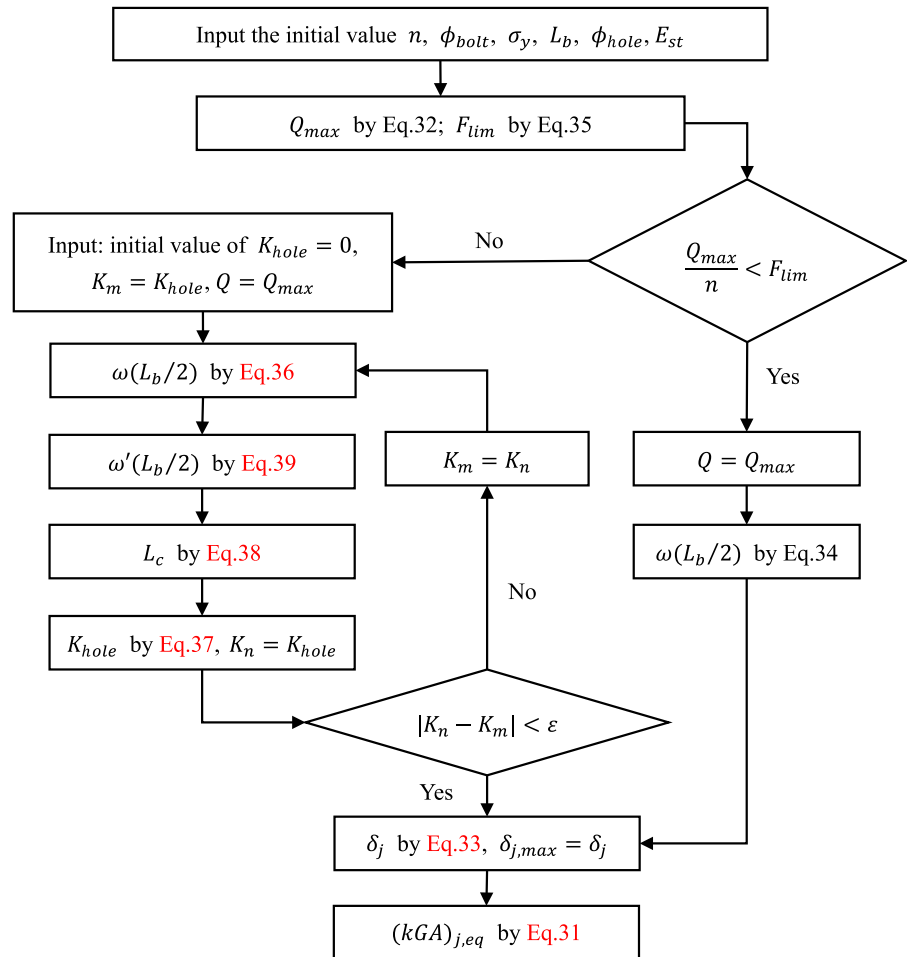


**Table 1** Parameters of investigation in the study

| Diameter of tunnel lining $D_e$ (m) | Thickness of lining (m) | Diameter of Bolt $\phi_b$ (mm) and cross section area | Normal force $N$ (MN) |
|---|---|---|---|
| 3.1 | 0.30 | 20 (245 mm$^2$) | 0 |
| 6.2 | 0.35 | 30 (561 mm$^2$) | 10 |
| 9.3 | | 33 (694 mm$^2$) | |

**Table 2** The combination of the number and diameter of bolts for the considered cases in the study

| $D_e$ (m) | $\phi_T$ (mm) | | |
|---|---|---|---|
| | 20 | 30 | 33 |
| 3.1 | 4Φ20 | 8Φ30 | 12Φ33 |
| 6.2 | 8Φ20 | 16Φ30 | 24Φ33 |
| 9.3 | 12Φ20 | 24Φ30 | 36Φ33 |

normal forces (Table 1). The combination of lining diameters and the assumed number of bolts is listed in Table 2; it aims to maintain the same number of bolts per meters along the circular profile. The yield stress of 32.4 MPa for the concrete and of 640 MPa for the steel of bolts were considered.

The curves of the moment varying the rotational angle of the joint are shown in Figs. 8, 9 and 10 respectively for the tunnel diameter of 9.3 m, 6.2 m, and 3.1 m based on different normal forces and bolting systems.

Figure 8 the curves can be divided into three sections with three different slopes when the normal force is equal to 10MN, and only two sections when the normal force is 0. The second section of the curve for 10MN normal force is almost parallel to the first section of 0MN, and the third section of the 10MN case is

**Fig. 8** The curve of the moment varying the rotational angle $\theta$ for an external lining diameter of 9.3 m and a thickness of 0.35 m, varying the applied normal force N and the bolting system
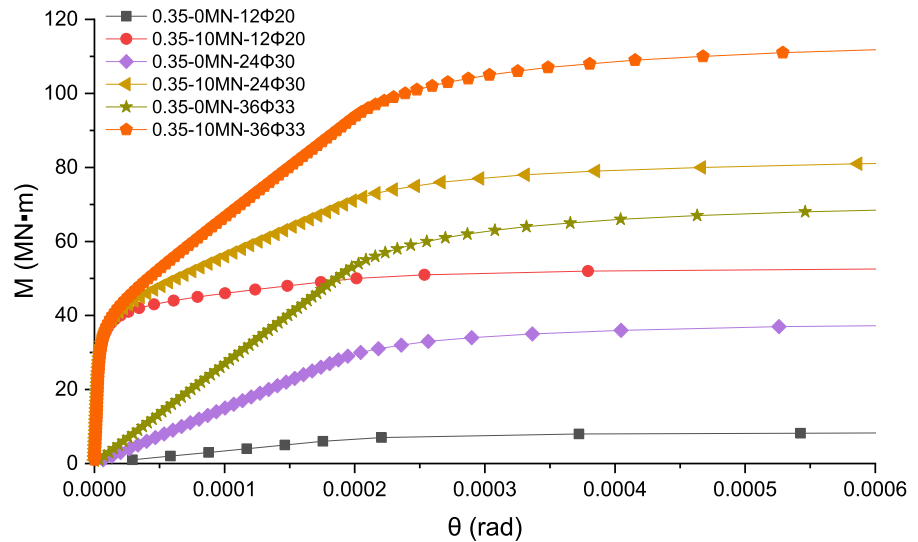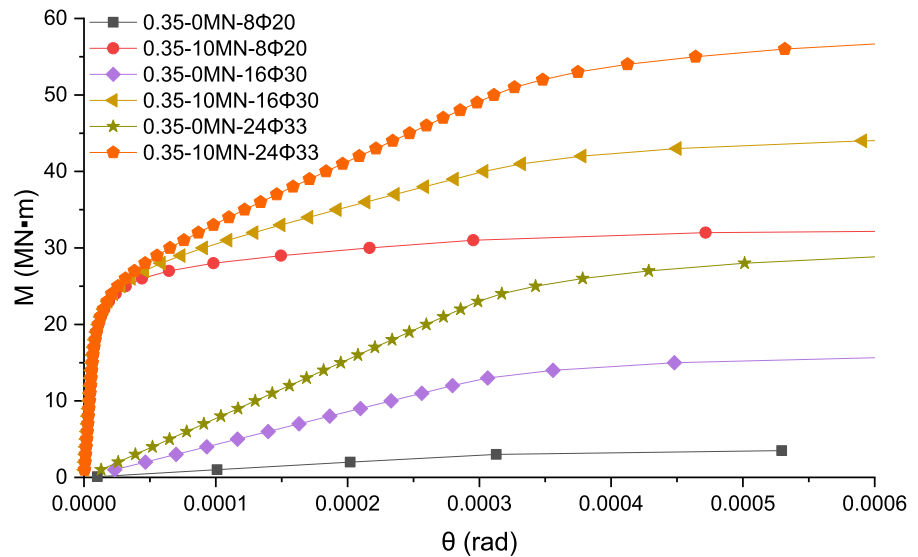


**Fig. 9** The curve of the moment varying the rotational angle $\theta$ for an external lining diameter of 6.2 m and a thickness of 0.35 m, varying the applied normal force N and the bolting system



also almost parallel to the second section of 0MN case, for each different combination of the bolting systems.

For the tunnel with a 6.2 m diameter and a 3.1 m diameter (Figs. 9, 10), the curves have a similar relationship between the 10MN and the 0MN case.

Referring to Fig. 8 for the case of N = 10 MN, it is possible to find that in the first section of the curve (joint closed, before the opening of the joint), the moment has a large change with the rotational angle (it means a high bending stiffness of the circular joint). After a transient and gradual decrease of the

slope, the second section practically have a constant slope (a constant bending stiffness). However, the slope in the second section varies with the adopted bolting system and has a larger value for the strong combination (36Φ33) with respect to the weak one (12Φ20). The curve in the third section is nearly parallel to the horizontal axis. Comparing the slopes of Figs. 8, 9 and 10, it is possible to note that the bending stiffness of the circular joint is mainly influenced by the tunnel diameter and the thickness before the joint opening, and the bending stiffness is additionally

**Fig. 10** The curve of the moment varying the rotational angle $\theta$ for an external lining diameter of 3.1 m and a thickness of 0.35 m, varying the applied normal force N and the bolting system
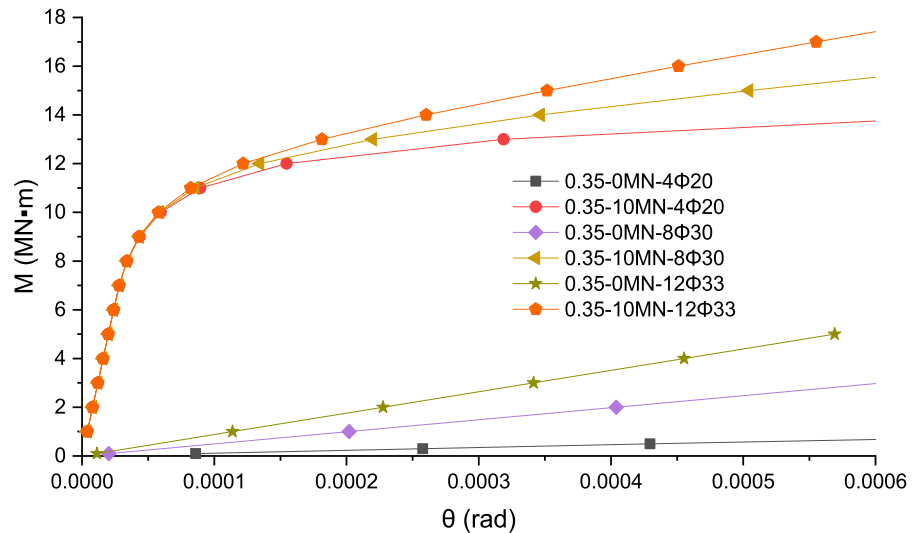


affected by the bolting system after that: the stronger bolt combination produces a larger bending stiffness after the joint opening.

### 3.2 Joint bending stiffness efficiency (JBSE) and a comparison with an indoor test result

Shiba et al. (1988) adopted the longitudinal bending stiffness efficiency (LBSE) to represent the deformation of a uniform beam compared to the beam with joints. In this paper, the joint bending stiffness efficiency (JBSE) is used to represent the ratio between the bending stiffness of the circular joint element with that of the lining rings.

$$\text{JBSE} = \frac{(EI)_{eq}}{E_{con}I} \qquad (40)$$

where the $(EI)_{eq}$ can be obtained by the second method shown in sect. 2.3 (Eq. 25).

On Eq. 25, the angle $\varphi$ is mainly determined by the ratio ($N/M$) between normal force and bending moment. The $\lambda$ parameter, $\lambda = N \cdot (D_e - t)/(M \cdot 4)$, is equal to 1 when the angle $\varphi$ is $-\pi/2$ (the case representing the joint closed and all its section compressed). According to the studied case of Sect. 3.1, the angle $\varphi$, $(1 - \sin\varphi)/2$ and the JBSE parameters varying with $\lambda$ are shown on Fig. 11, where $(1 - \sin\varphi)/2$ represents the relative locations of the neutral axis with respect to the lowest point along the vertical direction on the unit

circle (Fig. 11). From Fig. 11, the angle $\varphi$ decrease varying the parameter $\lambda$, and there is a nonlinear relationship between them. It is possible to note as the JBSE parameter shows a similar trend of the relative location of the neutral axis.

Considering the influence of the normal force, Li et al. (2019) carried out laboratory tests to analyse the longitudinal deformation under the combination of the normal force and the bending moment, and developed an analytical model of the bending stiffness; this model is able to add the normal force effect into the equation of the bending stiffness developed by Shiba et al. (1988). The comparison between the test results, the analytical solution from Li et al. (2019) and the proposed analytical model of Sect. 2.3 (second method) is shown in the Fig. 12. The adopted input parameters are shown in Table 3.

From Fig. 12, we can see how the general trend of the curve from the proposed model of this paper is similar to the one of the reference paper. This analytical results are lower than the test results and also than the analytical results of the reference paper when the $\lambda$ parameter is small; they approach to the test ones when the $\lambda$ parameter is close to 1. The main reason of this difference is that the bending stiffness evaluated in the reference paper is an equivalent value of the joint together with the segmental lining (LBSE), while the bending stiffness determined in this paper refers only to the circular

**Fig. 11** The angle $\varphi$, $(1 - \sin\varphi)/2$ and JBSE parameters varying with $\lambda = N \cdot (D_e - t)/(M \cdot 4)$
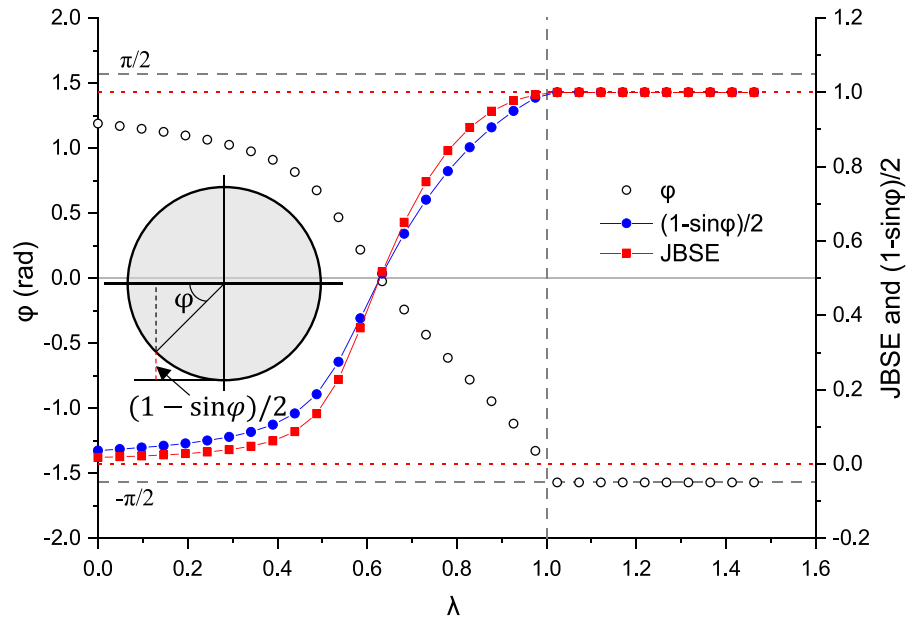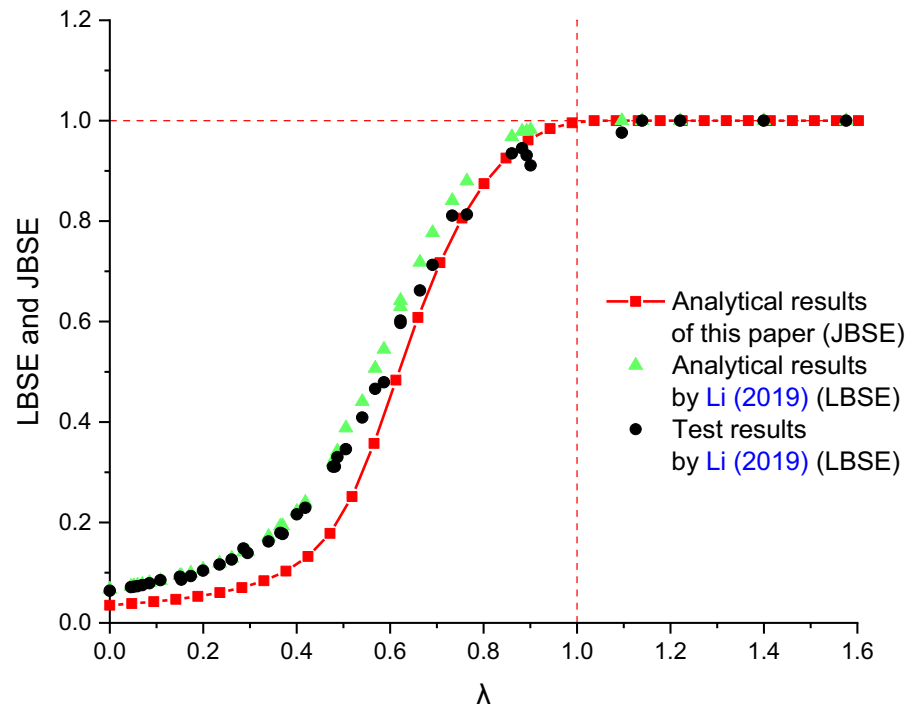


**Fig. 12** Comparison between the test and analytical results from the reference paper of Li et al. (2019) and the proposed solution of this paper based on Eqs. 25, 29, 30 and 40. Key: $\lambda = N \cdot (D_e - t)/(M \cdot 4)$



joint (JBSE). In order to simplify the calculation of the JBSE, a simplified equation of Joint bending stiffness efficiency ($JBSE_{Boltz}$) based on Boltzmann equation is derived (Appendix A).

### 3.3 The simplified equations of the bending stiffness of the joint element based on the Joint bending stiffness efficiency (JBSE)

Before the opening of the joint, its bending stiffness is the same of the lining ring, and can be calculated by using Eq. 6. The limit moment of the closed joint can be obtained by the following equation:

$$M_{lim,1} = \frac{N \cdot I}{A \cdot R_e} \tag{41}$$

After the opening of the joint, the bending stiffness of the joint element can be obtained by the following equation.

$$(EI)_{eq} = \mathrm{JBSE}_{Boltz} \cdot E_{con} \cdot I \tag{42}$$

where $\mathrm{JBSE}_{Boltz}$ is the simplified equation of JBSE based on Boltzmann equation which can be found on Appendix A.

When the bolt stress is close to the yield stress, there is a very small compression zone height. The limit moment can be obtained based on the yield stress of the bolt together with normal force N using a simplified approach (Appendix B):

$$M_{lim,2} = N \cdot (R_e - l) + (R_e - l + \frac{I}{A \cdot R_e}) \cdot \frac{\sigma_y}{2} \cdot n \cdot A_b \tag{43}$$

where $l$ is the height of the compression zone, and can be calculated by the following equation:

$$l = (1 - \sin\varphi) \cdot r + t/2 \tag{44}$$

the angle $\varphi$ is obtained by Eq. 29.

The limit moment $M_{lim,2}$ of the circular joint for the different cases considered in Sect. 3.1 when the normal force is 0MN and 10MN are obtained by Eq. 43 and using the integral approach (first method of Sect. 2.3). The results and the percent errors are listed in Table 4. The limit moments are influenced by the concrete yielding when the normal force is 10MN and the bolting systems are 8Φ30 and 12Φ33 for a tunnel diameter of 3.1 m; in the other cases the limit moment is influenced by the bolt yielding. Therefore Eq. 43 can be used to determine the joint limit situation when a circular joint reach the limit condition due to yielding of concrete or steel of bolts.

### 3.4 Shear stiffness of the circumferential joint

Referring to the considered cases of Sect. 3.1, the equivalent shear stiffness values are listed in Table 5

**Table 3** Adopted calculation parameters for the segmental lining and the bolting system in order to simulate the laboratory tests performed by Li et al. (2019)

| segment | | bolt | |
|---|---|---|---|
| External diameter (m) | 0.4 | Length (m) | 0.034 |
| Inner diameter (m) | 0.355 | Diameter (m) | 0.008 |
| Width of segment (m) | 0.065 | Number | 6 |
| Type of material | Plexiglass | Type of material | Polycarbonate |
| Elastic modulus (MPa) | 2.06 | Elastic modulus (MPa) | 2.41 |
| Poisson ratio | 0.3 | Poisson ratio | 0.32 |
| Density (g/cm³) | 1.18 | | |

**Table 4** The limit moment $M_{lim,2}$ (MN · m) of the circular joint obtained by using the Integral method (first method of Sect. 2.3) and the simplified equation (Eq. 43) for the considered cases of Sect. 3.1

| | Tunnel diameter (m) | 3.1 | | | 6.2 | | | 9.3 | | |
|---|---|---|---|---|---|---|---|---|---|---|
| | Bolting system | 4Φ20 | 8Φ30 | 12Φ33 | 8Φ20 | 16Φ30 | 24Φ33 | 12Φ20 | 24Φ30 | 36Φ33 |
| N = 0 | Integral method | 0.69 | 3.04 | 5.52 | 2.80 | 12.50 | 22.85 | 6.35 | 28.47 | 52.18 |
| | Equation 43 | 0.59 | 2.72 | 5.05 | 2.57 | 11.77 | 21.84 | 5.93 | 27.18 | 50.43 |
| | Percent error | 14.49% | 10.53% | 8.51% | 8.21% | 5.84% | 4.42% | 6.61% | 4.53% | 3.35% |
| N = 10 MN | Integral method | 13.99 | 15.97 | 17.70 | 31.14 | 40.31 | 50.24 | 49.86 | 71.18 | 94.21 |
| | Equation 43 | 13.35 | 15.48 | 17.80 | 29.70 | 38.90 | 48.97 | 47.44 | 68.69 | 91.94 |
| | Percent error | 4.57% | 3.07% | −0.56% | 4.62% | 3.50% | 2.53% | 4.85% | 3.50% | 2.41% |

**Table 5** The equivalent shear stiffness value for the considered cases of Sect. 3.1 and different bolting systems (gap between the hole and the bolt of 9 mm)

| $D_e = 3.1$ m | | $D_e = 6.2$ m | | $D_e = 9.3$ m | |
|---|---|---|---|---|---|
| Bolting system | Equivalent shear stiffness (MN) | Bolting system | Equivalent shear stiffness (MN) | Bolting system | Equivalent shear stiffness (MN) |
| 4Φ20 | 11.65 | 8Φ20 | 23.30 | 12Φ20 | 34.95 |
| 8Φ30 | 52.44 | 16Φ30 | 104.88 | 24Φ30 | 157.33 |
| 12Φ33 | 96.77 | 24Φ33 | 193.54 | 36Φ33 | 290.31 |

**Fig. 13** Equivalent shear stiffness of the circular joint for three different analysed bolting systems, varying the gap between the hole and the bolt, when the lining external diameter is 6.2 m
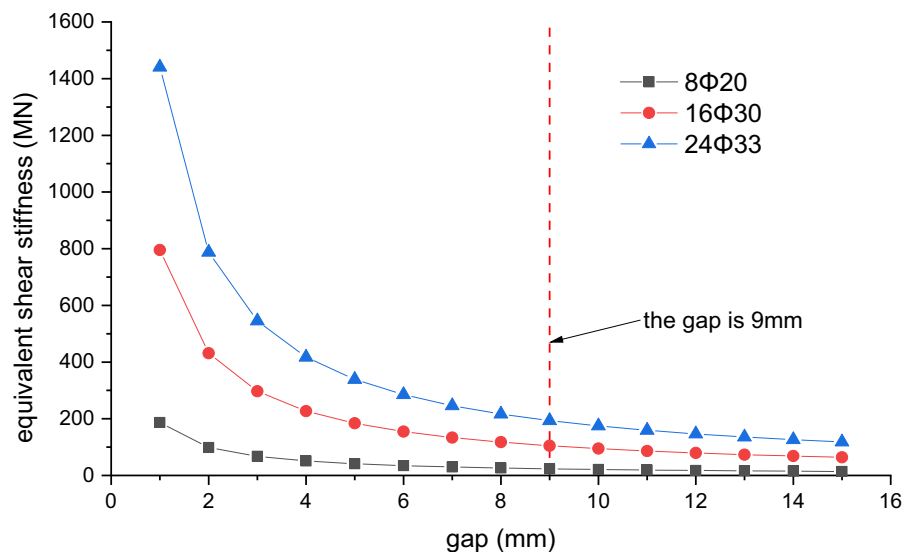


for different bolting systems when the gap between the hole and the bolt is equal to 9 mm.

From Table 5, it is possible to note how the bolting system has a great influence on the equivalent shear stiffness. Moreover the stiffness value has an obvious increase with the increase of the lining diameter and the number of bolts.

Besides of the bolts, the gap between the bolt and the hole also has a great influence for the shear deformation because the gap determines the free displacement space available for the bolt. The equivalent shear stiffness of a circular joint with different gap values for three different bolting systems is shown in Fig. 13 when the lining diameter is 6.2 m. In order to
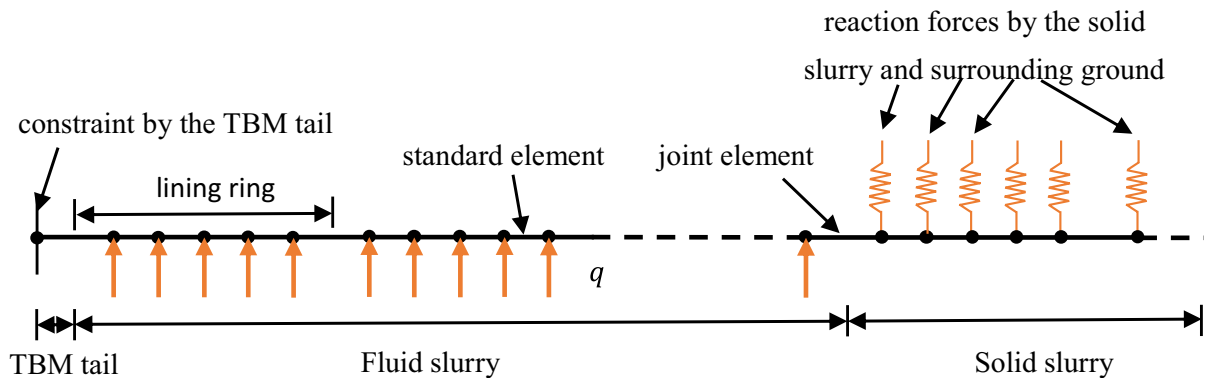
**Fig. 14** Standard elements and the joint elements used to simulate the tunnel segmental lining with the boundary constraints in the fluid slurry and in the solid slurry zones

show the exact trend, the equivalent shear stiffnesses are equal to 3579.36 MN, 8808.16 MN, 13,935.89 MN for the three combinations of bolts 8Φ20, 16Φ30, 24Φ33 respectively, when the gap is 0 (these values are also not show in the figure).

From Fig. 13, it is possible to see how the gap has a great influence on the shear stiffness for the analysed three different bolting systems. The curves show a nonlinear change with the increase of the gap. The decrease of the equivalent shear stiffness is large when the gap is very small, and the trend gradually becomes steady with the increase of the gap value.

## 4 Simulation of the circular joint in the numerical models

A FEM numerical model with the standard element which represent segmental rings and the joint element which represent circular joints, was adopted to simulate the longitudinal deformation based on the hyperstatic reaction method (Han et al. 2022). 4 standard elements

with a length of 20 cm and 1 joint element with a length of 40 cm are adopted to simulate a lining ring (Fig. 14).

The relationship between nodal displacements and nodal forces can be described by the following equation:

$$[K] \cdot [S] = [F] \tag{45}$$

where

$[S]$ is the matrix of nodal displacements, $[S] = \begin{bmatrix} S_1 & S_2 & S_3 & S_4 & \cdots & S_n & S_{n+1} \end{bmatrix}^T$; $S_i$ $(i = 1, 2, 3, \cdots, n+1)$ are the sub vectors of nodal displacements; $S_i = \begin{bmatrix} v_i & \theta_i \end{bmatrix}^T$, $v_i$ and $\theta_i$ are the vertical displacement and rotation angle of node $i$.

$[F]$ is the matrix of nodal forces, $[F] = \begin{bmatrix} F_1 & F_2 & F_3 & F_4 & \cdots & F_n & F_{n+1} \end{bmatrix}^T$; $F_i$ $(i = 1, 2, 3, \cdots, n+1)$ are the external forces applied on each node; $F_i = \begin{bmatrix} V_i & R_i \end{bmatrix}^T$, $V_i$ and $R_i$ are the transversal force and the bending moment of node $i$.

$[K]$ is the global stiffness matrix and is composed by the local stiffness matrices of each element, assembled through the overlapping terms along the diagonal.

$$[K] = \begin{bmatrix} k_{1,a} & k_{1,b} & 0 & 0 & \cdots & 0 & 0 \\ k_{1,c} & k_{1,d}+k_{2,a} & k_{2,b} & 0 & \cdots & 0 & 0 \\ 0 & k_{2,c} & k_{2,d}+k_{3,a} & k_{3,b} & \cdots & 0 & 0 \\ 0 & 0 & k_{3,c} & k_{3,d}+k_{4,a} & \cdots & 0 & 0 \\ \vdots & \vdots & \vdots & \vdots & \ddots & 0 & 0 \\ 0 & 0 & 0 & 0 & \cdots & k_{n-1,d}+k_{n,a} & k_{n,b} \\ 0 & 0 & 0 & 0 & \cdots & k_{n,c} & k_{n,d} \end{bmatrix} \tag{46}$$

where $k_{i,a}$, $k_{i,b}$, $k_{i,c}$, $k_{i,d}$ are the $2 \times 2$ stiffness sub matrices of each elements, which can be obtained by equally dividing the following local stiffness matrix:

$$[k_E]_i = \frac{EI}{l^3} \begin{bmatrix} \overbrace{\begin{matrix} \frac{12}{1+\Phi} & \frac{6l}{1+\Phi} \\ \frac{6l}{1+\Phi} & \frac{4+\Phi}{1+\Phi}l^2 \end{matrix}}^{[k]_{i,a}} & \overbrace{\begin{matrix} -\frac{12}{1+\Phi} & \frac{6l}{1+\Phi} \\ -\frac{6l}{1+\Phi} & \frac{2-\Phi}{1+\Phi}l^2 \end{matrix}}^{[k]_{i,b}} \\ \underbrace{\begin{matrix} -\frac{12}{1+\Phi} & -\frac{6l}{1+\Phi} \\ \frac{6l}{1+\Phi} & \frac{2-\Phi}{1+\Phi}l^2 \end{matrix}}_{[k]_{i,c}} & \underbrace{\begin{matrix} \frac{12}{1+\Phi} & -\frac{6l}{1+\Phi} \\ -\frac{6l}{1+\Phi} & \frac{4+\Phi}{1+\Phi}l^2 \end{matrix}}_{[k]_{i,d}} \end{bmatrix} \quad (47)$$

where the ratio $\Phi$ between the bending stiffness and the shear stiffness is adopted to consider the influence of the shear deformability of the numerical elements. The ratio $\Phi$ can be obtained by the following equation:

$$\Phi = \frac{12 \cdot (EI)}{(kGA) \cdot l^2} \quad (48)$$

where $(EI)$ is the bending stiffness, $(kGA)$ is the shear stiffness.

The first ring in the TBM tail is constrained by the shield tail brush, and the other rings outside the shield are constrained by the surrounding slurry and ground (Fig. 14). Therefore, the endpoint of the first joint element has a nill transversal displacement and rotation.

Due to the gap presence between the segmental lining and the ground, a synchronous grouting is used to fill it during the construction phase. Because of the long setting time of the single component slurry, the buoyancy phenomenon of the lining and its uplift develop in the fluid slurry zone (Zhou and Ji 2014). Based on the Archimedes' principle, the buoyancy load $q$ which is applied on the segmental lining by the slurry is equal to the specific weight of slurry multiplied to the total volume of the lining ring reduced by the weight of the lining. Considering the low viscosity of slurry at the initial stage and the extreme small upward displacement velocity of lining rings, the resistance from the slurry to the lining ring movement is small and can be neglected.

$$q = \gamma_{sl} \cdot \frac{\pi}{4} \cdot D_e^2 - \gamma_{con} \cdot \frac{\pi}{4} \cdot \left[ D_e^2 - \left( D_e - 2t \right)^2 \right] \quad (49)$$

where $\gamma_{sl}$ and $\gamma_{con}$ are the specific weight of slurry and concrete respectively.

The length of the fluid slurry zone depends on the advancement speed of TBM and the setting time of the slurry. The speed relies on the excavation time and the assembling time of the lining ring. The hardening time can be tested by an indoor test, for example, and it is equal to the time from mixing to reach a specific value of penetration resistance (0.5 MPa) by the penetration resistance method (Chinese Specification JGJ/T 70-2009) (China, 2009). So, the length of the fluid slurry zone can be obtained by the following simple equation:

$$d = v \cdot t_0 \quad (50)$$

where $v$ is the gross average speed of TBM, $t_0$ is the hardening time of the slurry.

During the slurry hardening process, the viscosity and the strength increase with the time and the resistance produced by the surrounding slurry and ground to the segmental lining movement becomes a main external force after the slurry hardening.

Winkler springs are often used to represent the interaction between the ground and the lining (Oreste 2013). Vertical Winkler springs are adopted to reflect the reaction of the hardened slurry and ground on the segmental lining due to the vertical displacement of lining rings. The external force of the spring is considered through an adding term $[k_w]_{i,a}$ in the global stiffness matrix $[K]$ (Oreste 2007):

$$[k_w]_{i,a} = \begin{bmatrix} k_w \cdot l_{av,i} & 0 \\ 0 & 0 \end{bmatrix} \quad (51)$$

where $l_{av,i}$ is the average length of the element length on the both sides of the node $i$, $k_w$ is the spring stiffness due to the ground and slurry and can be obtained by the following equation:

$$k_w = q_u / \delta_u \quad (52)$$

where $\delta_u$ is the ultimate displacement of the tunnel lining; according to the results by Gong et al. (2018), it is equal to $0.02 \cdot D$ when the tunnel has a small depth from the surface; $q_u$ is the ultimate pressure of slurry and ground, and can be obtained as:

$$q_u = D_e \cdot h_0 \cdot \gamma_G - \frac{\pi}{8} D_e^2 \cdot \gamma_G \quad (53)$$

**Fig. 15** The JBSE parameter along the segmental lining (starting from the TBM tail) with different normal force values applied by the TBM, for the analysed case of the Metro line of Ningbo in China
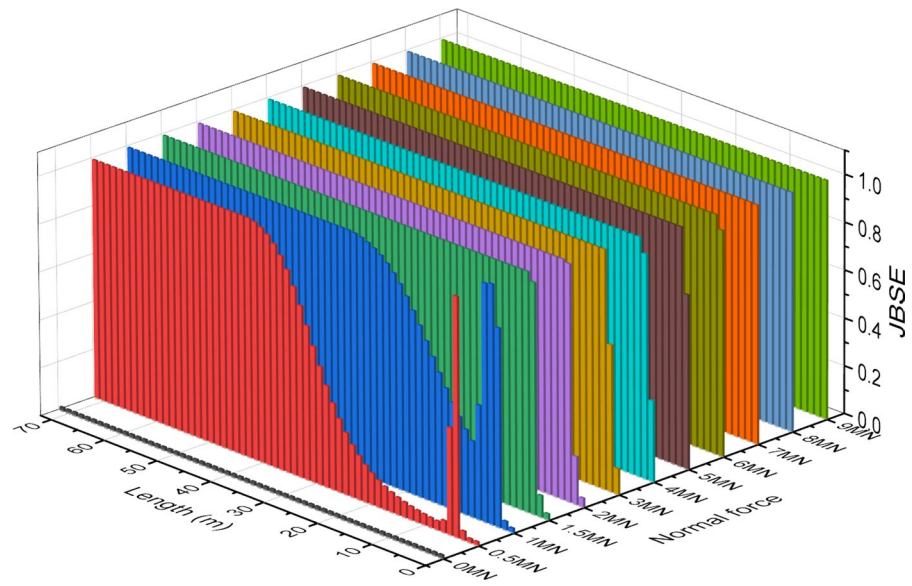


where $h_0$ is the tunnel axis depth from the surface, $\gamma_G$ is the ground bulk density.

On the developed specific numerical model, an iterative procedure is adopted due to the dependency of the bending stiffness of the joint element on the moment and the normal force. The iterative procedure requires the following steps:

**Step 1**: calculation of the moment $M_1$ along the segmental lining considering the JBSE parameter of all the circular joints equal to 1;

**Step 2**: based on the results of the moment $M_1$ in the first step, calculation of the bending stiffness of all the joints, and obtaining the new moments $M_2$; the mean $\overline{M_2}$ of the two moments is then calculated;

**Step 3**: calculation of the new bending stiffness and the moments $M_{i+1}$ based on the last average moment $\overline{M_i}$ of the previous steps ($i = 2, 3, 4 \dots$);

**Step 4**: comparison of the moments $M_{i+1}$ with the average moments $\overline{M_i}$, calculation of the mean $\overline{M_{i+1}}$ of the two moments; when the largest difference among the joints is larger than a specific value, go back to the step 3 with $i = i + 1$; otherwise, end of the iterative process.

The stiffness of the circular joint is weaker than that of the lining ring, and it influences the longitudinal deformation of the lining under the application of the buoyancy forces and the jack thrust by the TBM tail. How the stiffness of the circumferential joint impact the deformation of the segmental lining is discussed in the following section.

In the Sect. 3 it was possible to verify how the bolting system, the geometry of the tunnel lining and the materials characteristics (concrete and steel bolts) have a significant effect on the equivalent bending stiffness of the circular joint. In addition, the normal force has also an important influence for the bending deformation along the longitudinal direction. Because the normal force is variable during the construction phase, its effect is discussed firstly in this section. Moreover, the gap between the hole and the bolt is a critical parameter for determining the equivalent shear stiffness of the joint (Sect. 2.4). The influence of the equivalent shear stiffness is analysed in the second part of the section.

### 4.1 Influence of the normal force

The segmental lining and the bolt system adopted in the case of the Metro tunnel of Ningbo in China has been described in Sect. 3.1. In addition, the slurry is made up of cement, bentonite, sand, fly ash, quick lime, water and admixture, of which the quantity proportion is as follows: 150:300:2750:650:100:900:1. The hardening time of the adopted slurry is about 15 h (Zhou and Ji 2014). The average construction speed is about 0.4–0.5 m/h (the value of 0.5 m/h is considered in the analysis) (Chen et al. 2018). Because the diameter of shield tail of the TBM is equal to 6.34 m, the gap between the segmental lining

**Fig. 16** Measured (maximum value) and calculated vertical displacement of the segmental lining with different normal forces for the case of the Metro line of Ningbo in China
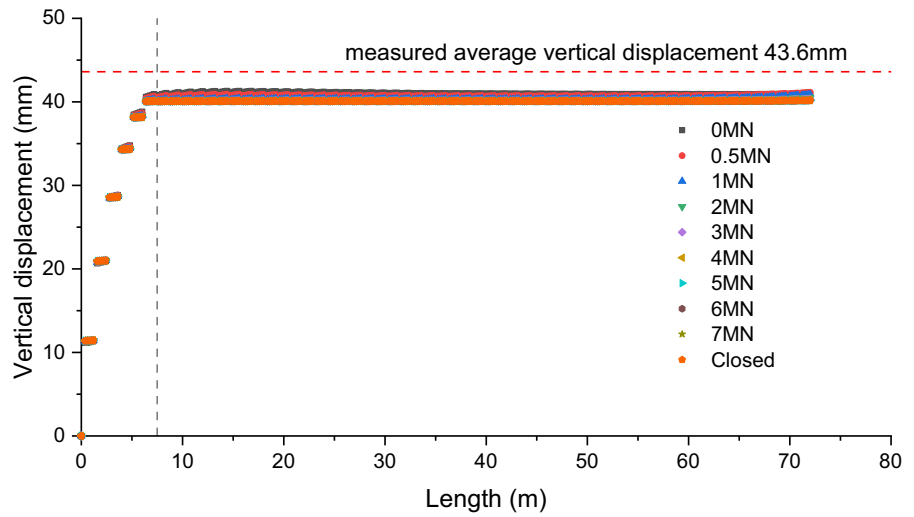


**Fig. 17** The calculated value vertical displacement gradient of the segmental lining in the circular joints with different normal forces for the case of the Metro line of Ningbo in China
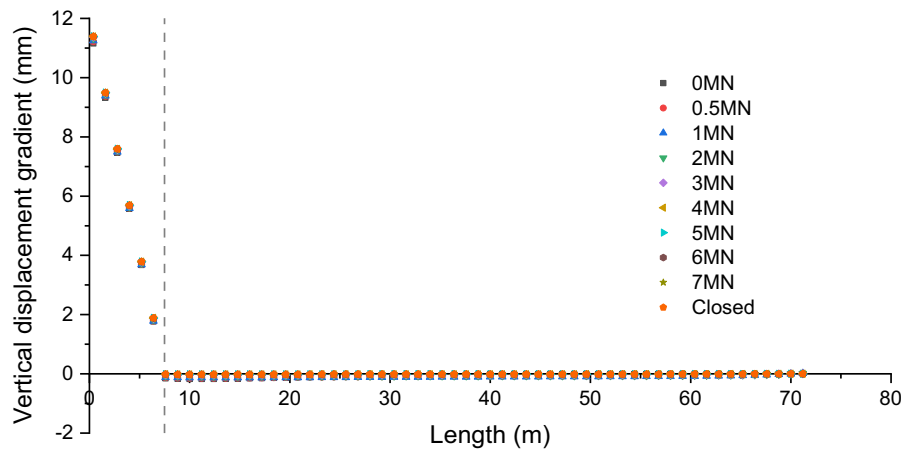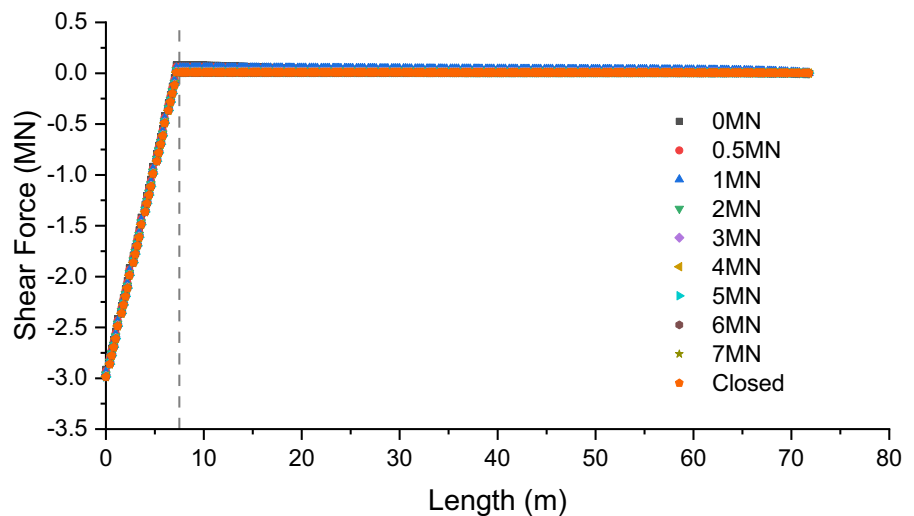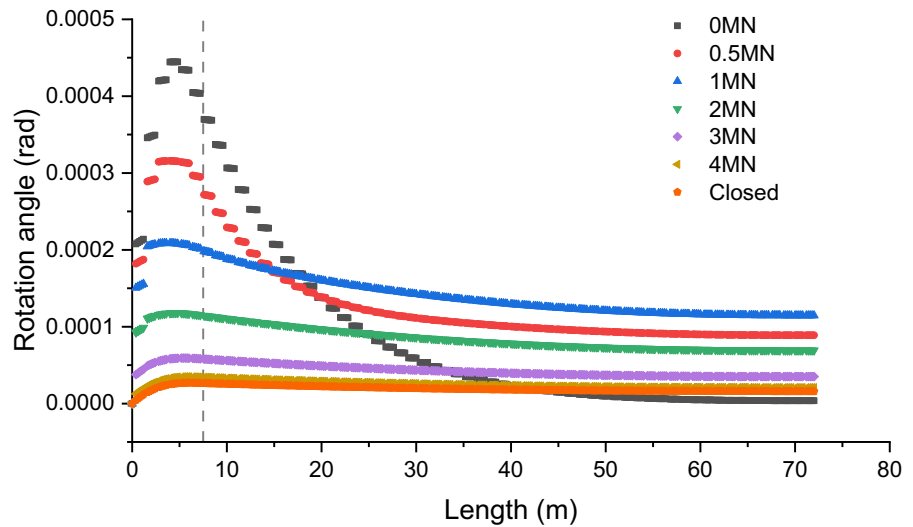


**Fig. 18** The calculated value of the shear force of the segmental lining with different normal forces for the case of the Metro line of Ningbo in China

**Fig. 19** The rotation angle of the segmental lining with different normal forces for the case of the Metro line of Ningbo in China



and the ground wall is equal to 70 mm. The tunnel depth from the surface is about 15 m.

Based on the developed longitudinal deformation model (Fig. 14) and the proposed iterative procedure, the vertical displacement, the shear force, the rotation angle, and the moment of the segmental lining along the longitudinal direction is calculated and shown in Figs. 16, 17, 18, 19, 20 and 21. In order to consider the influence of the joint state, the longitudinal deformation is calculated when the normal force is equal to 0, 0.5, 1, 1.5, 2, 3, 4, 5, 6, 7, 8 and 9MN, separately. All the joints are open when the normal force is equal to 0MN, and all of them are closed when the

normal force is equal to 8MN and 9MN. Because the JBSE can represent the joint state, the JBSEs along the longitudinal direction are shown on Fig. 15 varying the normal force. When the normal force is equal to 0.5MN and 1MN there are a lot of joints open (the fourth and fifth joint have a high value of JBSE because the moment is close to 0). When the normal force is equal to 1.5MN and 2MN, the first three joints are open; only the first two joints are open when the normal force is 3MN and 4MN. With the increase of the normal force, the joints of the segmental lining tend to close.

**Fig. 20** The relative rotation angle of the circular joints with different normal forces for the case of the Metro line of Ningbo in China
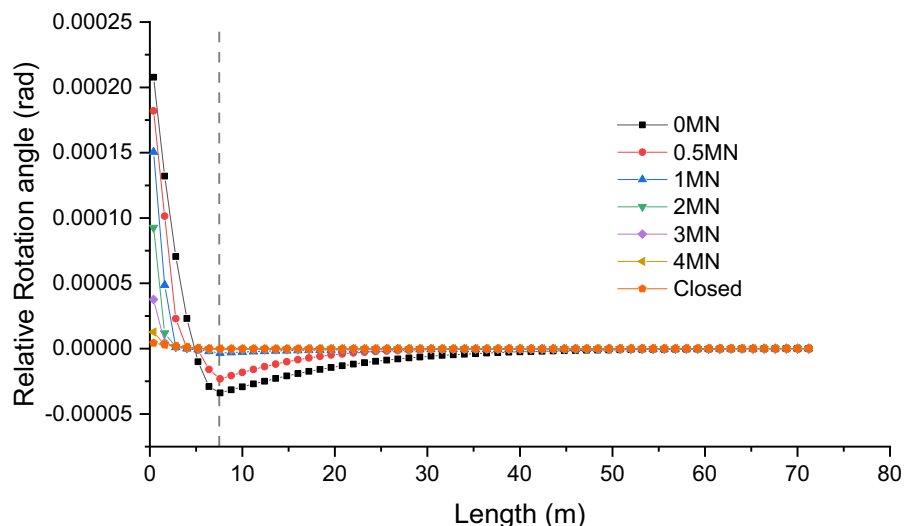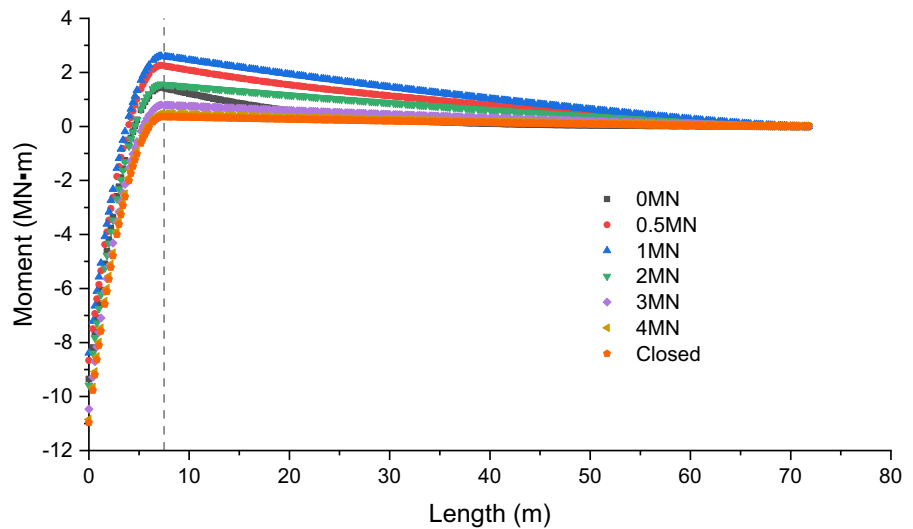
**Fig. 21** The moment of the segmental lining with different normal forces for the case of the Metro line of Ningbo in China
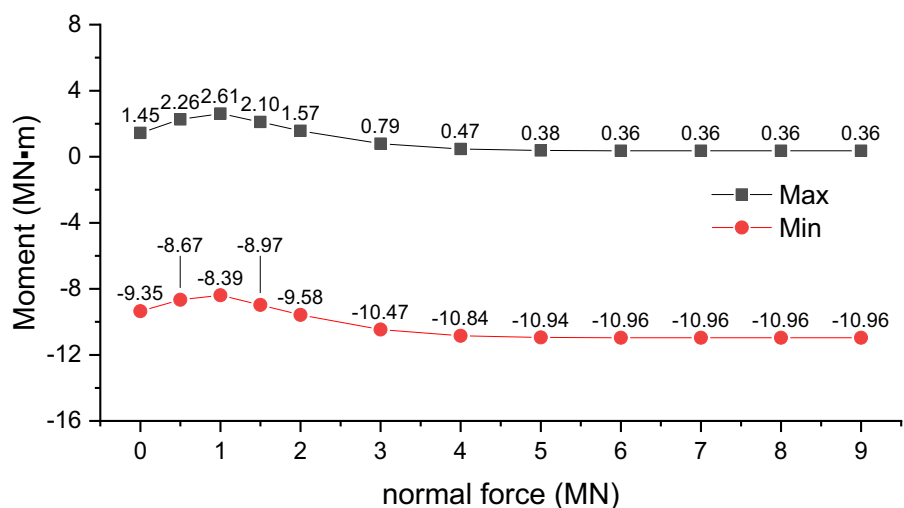


The monitoring of the vertical displacements (Zhou and Ji 2014) shows a maximum value of about 43.6 mm for this type slurry. From Fig. 16, it is possible to see how the calculated maximum vertical displacement (41.3 mm when the normal force is 0MN) is approximate to the measured value (43.6 mm).

Based on the vertical displacements trend, the gradient of the vertical displacements in the circular joints was calculated and it is shown in Fig. 17. In the fluid slurry zone (for a distance of 7.5 m from the TBM tail), the vertical displacement grows up with the increase of the distance from the TBM tail, but its gradient shows a decreasing trend. In the solid slurry zone, the vertical displacements keep steady; also the

shear force (Fig. 18) has its maximum negative value at the TBM tail and tends to zero at the dividing line between the fluid and the solid slurry zone. The first circular joint has the maximum vertical displacement gradient and the maximum negative shear force: therefore particular attention must be paid to this zone of the segmental lining.

From Fig. 19 it is possible to note how the rotation angle (referring to a horizontal plane) of the segmental lining along the longitudinal direction undergoes an increase followed by a decrease, and the turning point occur close to the dividing line. Furthermore, the rotation angle mainly depends on the rotation of the joint. Different values of the rotation angle can

**Fig. 22** The maximum positive and negative moments of the segmental lining with different normal forces for the case of the Metro line of Ningbo in China
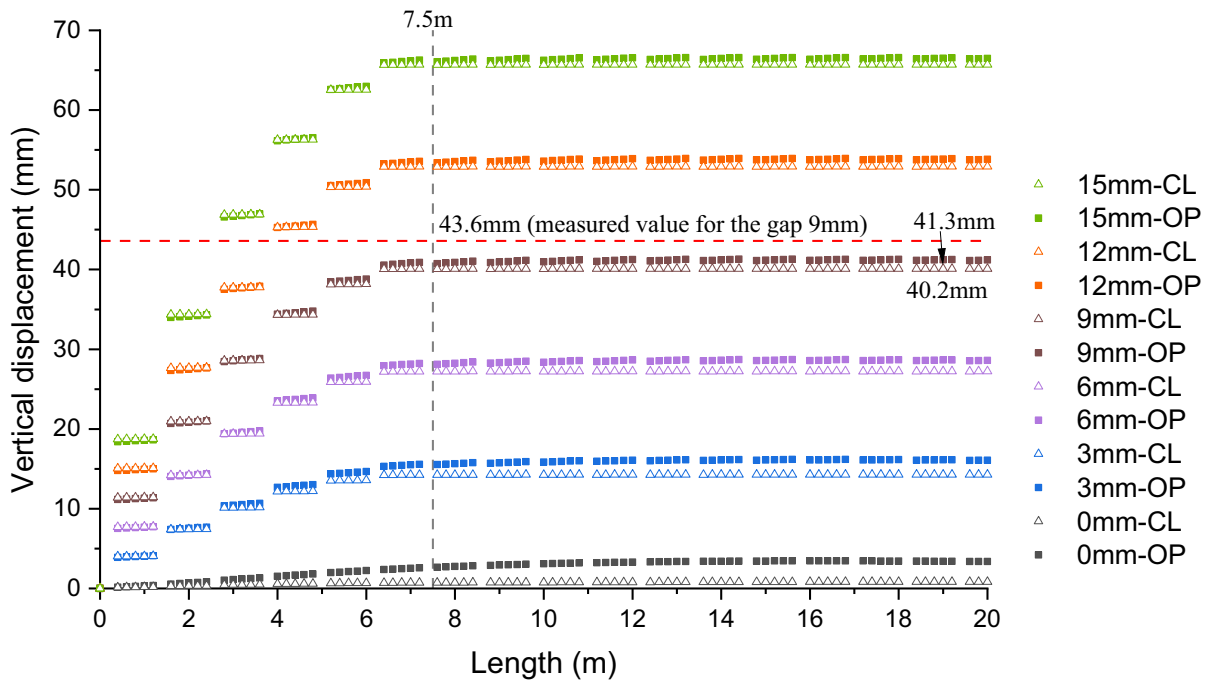
**Fig. 23** Comparison of the vertical displacements calculated by the developed FEM model with the measured values, for a slurry with 15 h hardening time at the studied case of the Metro line of Ningbo in China. Key: 15 mm-OP means the gap is equal to 15 mm and the normal force is 0MN (joint open); 6 mm-CL means the gap is equal to 6 mm and the normal force is 10MN (joint closed); 7.5 m is the length of the dividing lines between the fluid slurry and the solid slurry zones

be seen varying the normal force. The relative rotation angle of the circular joint is calculated from the rotation angle evaluated along the segmental lining (Fig. 20): the maximum and the minimum values of the relative rotation angle show an increasing trend with the decrease of the normal force; moreover, the relative rotation angle has a good consistency with the moment trend. The maximum value and the minimum one of the relative rotation angles are reached at the first joint and at the joint close to the dividing line, respectively; on the other hand, the maximum negative moment is reached at the first joint, and the maximum relative rotation angle also occurs at the first joint. Therefore, when it is necessary the evaluation of the damage risk of a segmental lining, the first joint and the one close to the dividing line are the critical ones.

In Fig. 21 the bending moment trend for different applied normal forces is shown; an obvious influence of the normal force on the moment is seen. The maximum positive and negative moment of the segmental lining with different normal force are shown

in Fig. 22. Due to the effect of the joint state, the relationship between the moment and the normal force is of a nonlinear type. An interesting phenomenon can be seen: the maximum moments increase with the normal force when the normal force is smaller than 1MN, and then they decrease with increasing the normal force when the normal force is larger than 1MN.

In conclusion, the first circular joint close to the TBM tail needs to be investigated carefully for its shear deformation and the developed rotation; in addition, the joint close to the dividing line between the fluid and solid slurry zones is another high-risk joint due to the relative rotation. The normal force has a slight effect on the shear deformation, but has a significant influence on the rotation.

### 4.2 Influence of the gap between the hole and the bolt

In order to know the influence of the shear stiffness of the circular joint on the deformation of the tunnel lining, the vertical displacement for 7 different values

**Fig. 24** Curves of the equivalent shear stiffness of the circular joint and of the maximum vertical displacement of the lining varying the gap between the bolt hole and the bolt for the case of the circular joint closed (axial force N = 10MN) and open (N = 0)
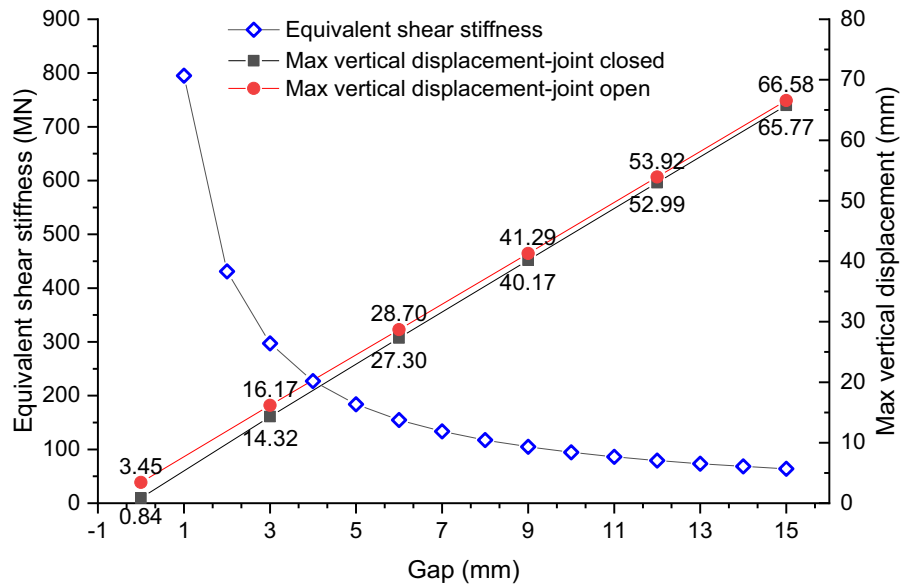


of the gap between the bolt hole and the bolt is calculated and compared with the test results when the joint is open and closed (Fig. 23). Based on the calculation results previously presented, all the joints are open when the normal force is equal to 0, and all the joints are closed when normal force is 10MN.

Based on the results of Fig. 23, when the gap is equal to 9 mm (adopted in the studied case of Ningbo Metro line tunnel) the calculated values are close to the on-site measured ones. Compared with the continuous beam model, the proposed model can show the displacements of the segmental lining and of the circular joints respectively, and make it possible to analyse the exact stress condition of the most dangerous joint, that one having the highest value of deformation.

The differences of the vertical displacements between the two considered normal forces for every gap value are very small when the segmental ring is close to the shield tail, and they become larger with the increase of the distance from the shield tail. The differences are very small when the gap is large, but they become larger when the gap is small. The vertical displacements for each of 7 gap values have the same trend, increasing along the longitudinal direction. In order to show the relationship among these curves, the maximum value of the vertical displacements with different gap values and the equivalent shear stiffness of the circular joint is shown in

Fig. 24. The equivalent shear stiffness when the gap is 0 (8808.16 MN) is not shown in the figure.

A very interesting phenomenon can be seen from Fig. 24: the maximum vertical displacement has a linear increase with the gap, while the equivalent shear stiffness has a nonlinear decrease. It means that the change of the equivalent shear stiffness is very small with the increase of the gap when the gap is large, while the increase of the maximum vertical displacement remains large. Based on this statement, trying to reduce the gap between the bolt hole and the bolt is always a key point that can be used to decrease the upward vertical displacements of the segmental lining due to the buoyancy phenomenon.

The shear force trend along the longitudinal direction is similar to that of Fig. 18 where the maximum negative value is at the first joint and the maximum positive value at the one near the dividing line between the fluid slurry and the solid slurry zone; the influence of the gap for the maximum and minimum shear force is shown in Fig. 25. The shear stiffness and the gap value show a small influence on the maximum negative and positive shear force values.

Moreover, the influence of the shear stiffness on the bending moment due to the difference of the gap between the bolt hole and the bolt is shown in Figs. 26 and 27 (the figures display one nodal value every 5 nodes). When the normal force is equal to 0MN (it means that all the joints are open and the

**Fig. 25** The influence of the gap between the bolt hole and the bolt on the maximum positive and negative shear force values for the studied case of the Metro line of Ningbo in China. Key: OP: circular joint open (axial force N = 0); CL: circular joint closed (N = 10MN); Max: maximum positive value of the shear force along the tunnel lining; Min: maximum negative value of the shear force
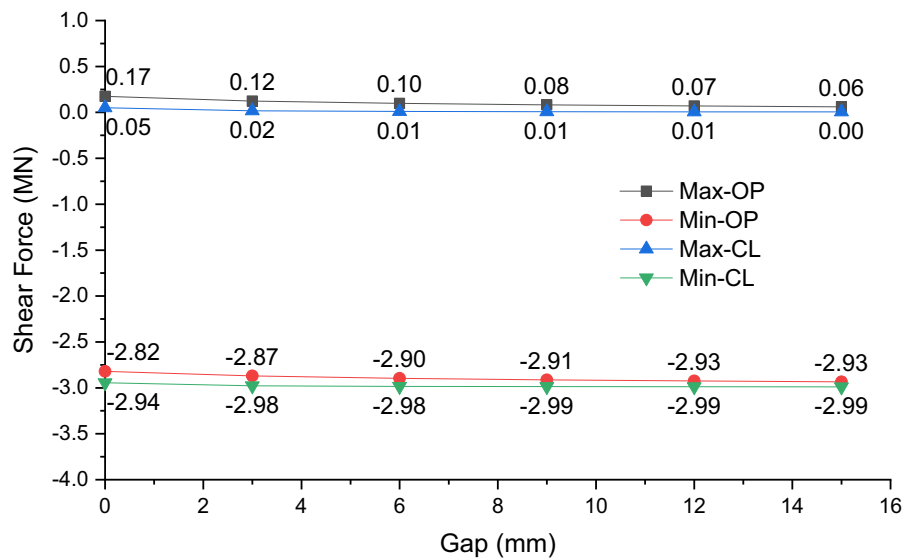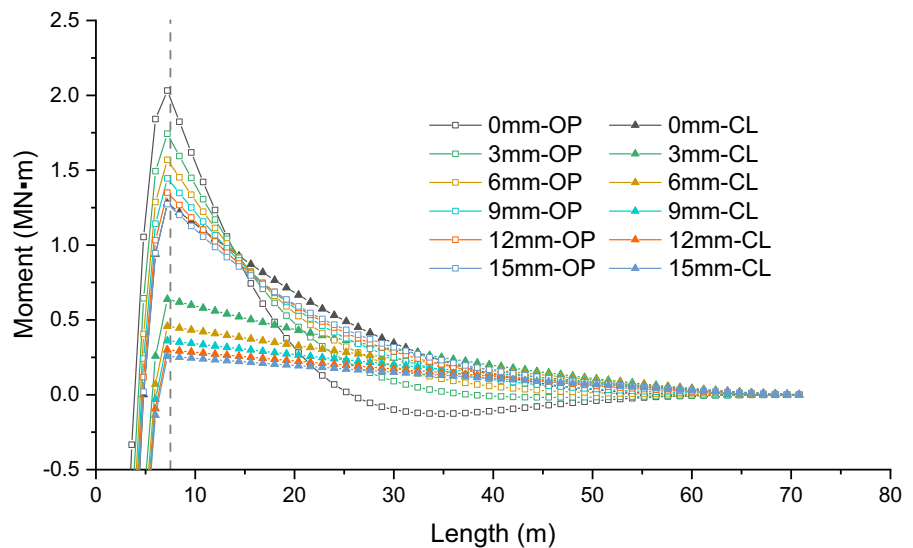
**Fig. 26** Influence of the gap between the bolt hole and the bolt on the moments along the longitudinal direction for the studied case of the Metro line of Ningbo in China. Key: OP: circular joint open (axial force N = 0); CL: circular joint closed (N = 10MN); 0–15 mm: the gap value

bending stiffness is equal to 16,883.53 MN · m², the maximum negative moment is reached when the gap is equal to 15 mm (the shear stiffness is 63.92 MN), but the maximum positive moment occurs when the gap is 0 mm (the shear stiffness is 8808.16 MN). There are similar results when the joints are closed (the normal force is 10MN and the bending stiffness is equal to the one of the concrete segmental lining, 952,722.48 MN · m²). From Figs. 26 and 27 it is possible to note how the larger shear stiffness (smaller gap value) causes a more dramatic fluctuation of the

moments along the longitudinal direction. The presence of the normal force is able to reduce the fluctuation level of the moments, but also to increase the maximum negative value.

## 5 Conclusions

Lining rings which are composed of segments that are connected by circular bolts, constitute the support of tunnel when a Tunnel Boring Machine (TBM) is

**Fig. 27** Influence of the gap between the bolt hole and the bolt on the maximum positive and negative moments along the longitudinal direction for the studied case of the Metro line of Ningbo in China. Key: OP: circular joint open (axial force N = 0); CL: circular joint closed (N = 10MN); Max: maximum positive value of the moment along the tunnel lining; Min: maximum negative value of the moment
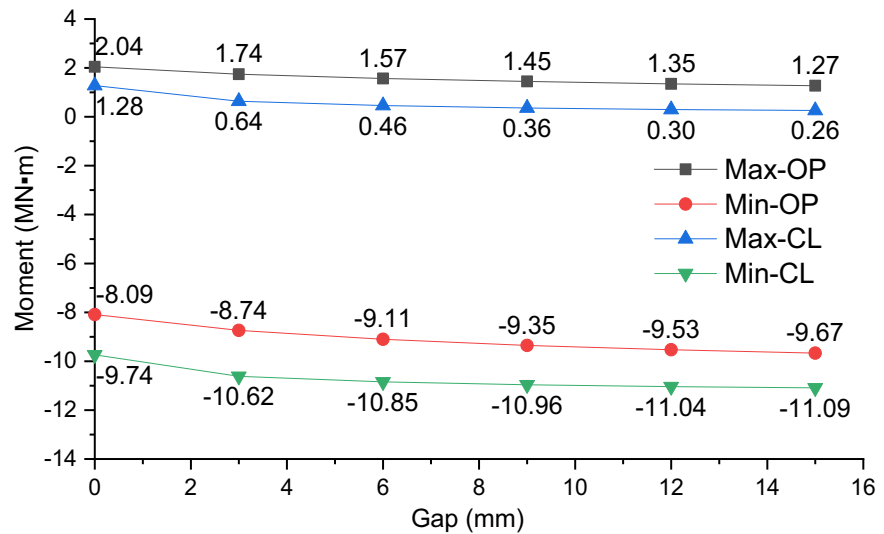


adopted for the excavation. Lining rings are also connected by longitudinal bolts along the tunnel axis. The circular joints of the lining are weaknesses when a deformation develop along the tunnel axis under the application of the jack thrust by the TBM tail and of transversal loads to the lining.

A filling material (slurry) is injected in the space between the lining and the tunnel wall. Due to the variation of its mechanical characteristics over time, a fluid slurry zone and a solid slurry one can be seen along the segmental lining starting from the TBM tail. Where the slurry is fluid, a buoyancy force is applied to the segmental lining and it produces upward displacements of the lining rings. In addition, the cycle of excavation and segment assembly cause a fluctuating jack thrust. This uneven and variable force leads to longitudinal deformations and stress concentrations; they result in a risk of damage of the tunnel lining during the construction phase.

Considering the importance and complexity of the evaluation of the circular joint stiffnesses, a joint model including the compression zone and the equivalent tension zone is developed. On the basis of this model, the compressive stiffness and the tensile stiffness for the two specified zones in the joint is derived. According to these stiffnesses, a new bending stiffness equation of the joint is obtained, and a numerical procedure is developed, which is able to

consider the yielding of each point of concrete and of the longitudinal bolts. Furthermore, a new shear stiffness equation of the joint is determined in accordance with the bolt bending deformation of the bolt and with the constraint produced by the hole wall to the bolt. Thanks to the new bending stiffness and the shear stiffnesses of the circular joints, the deformation of the joints and of the segmental rings can be considered separately. This model allows to evaluate in detail all the aspects that involve the behavior of segments and circular joints along the longitudinal axis of the tunnel lining.

Based on the developed numerical procedure, the bending deformation under the combination of the normal force and the moment is evaluated considering the influence of the diameter of the tunnel lining, the thickness of the lining, the combination of bolts and the applied normal force. A comparison of the calculated results with the available laboratory results and in situ measurements was developed, showing a good consistency.

From the obtained results, it was possible to note that the shear force that develops along the lining following the application of the buoyancy forces is not influenced by the normal force applied by the TBM jacks. While, the maximum bending moments (in absolute value) are obtained for a normal force value higher than a certain value (4MN) and for

**Fig. 28** The comparison of the Boltzmann function (Boltzmann fitting) and the modified Boltzmann equation (JBSE Boltz equation) with the calculated value of JBSE for the case of Metro line of Ningbo in China, varying with $\lambda$ parameter
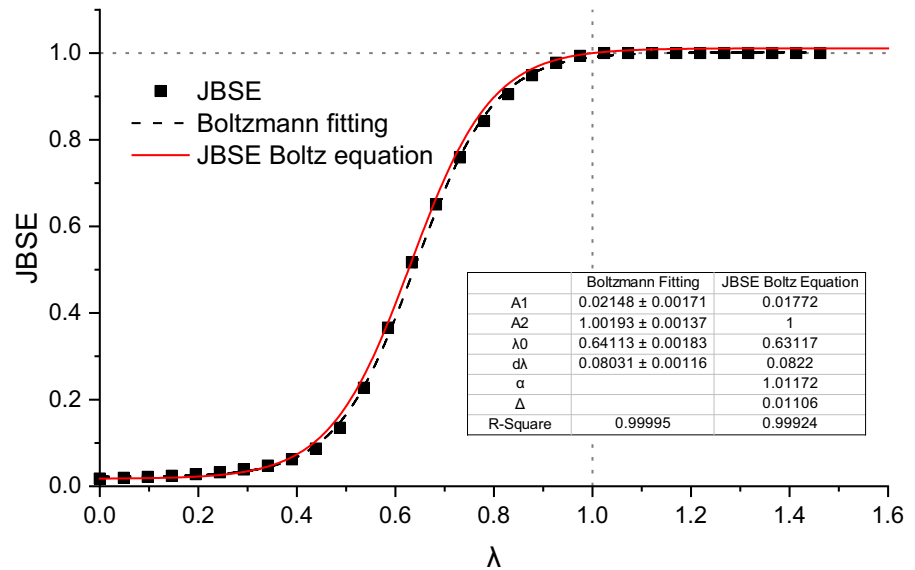


|  | Boltzmann Fitting | JBSE Boltz Equation |
|---|---|---|
| A1 | 0.02148 ± 0.00171 | 0.01772 |
| A2 | 1.00193 ± 0.00137 | 1 |
| λ0 | 0.64113 ± 0.00183 | 0.63117 |
| dλ | 0.08031 ± 0.00116 | 0.0822 |
| α |  | 1.01172 |
| Δ |  | 0.01106 |
| R-Square | 0.99995 | 0.99924 |

**Fig. 29** Height of the compression zone for the examined 6 cases (different axial forces N and bolting systems) based on the Sect. 3.1, varying the bending moment M. Key: the values 3, 13, 24, 32, 42, 52 MN · m at the end of the represented arrows are the moments when the highest bolt begins to yield
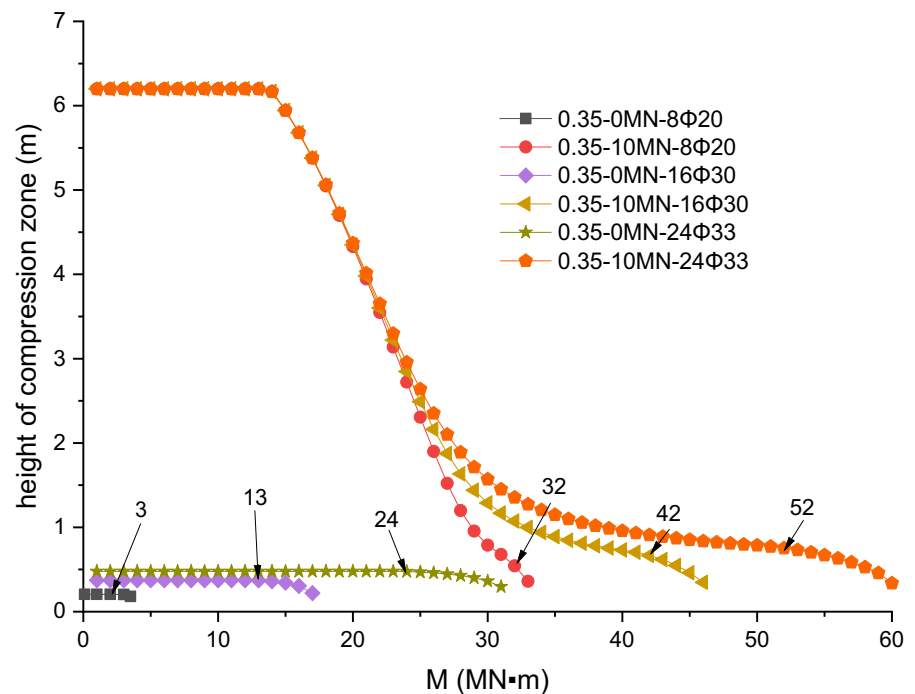


values of the gap between the bolt hole and the bolt used to connect the lining rings higher than 5 mm. The maximum displacements of the segmental lining occur in the presence of the greatest values of the gap.

During the design phase, the significant increasement of the shear force and the moment on the first joint behind the shield tail caused by the buoyancy of the slurry need to be checked. The model on the Sect. 4 can be an option to evaluate the segmental
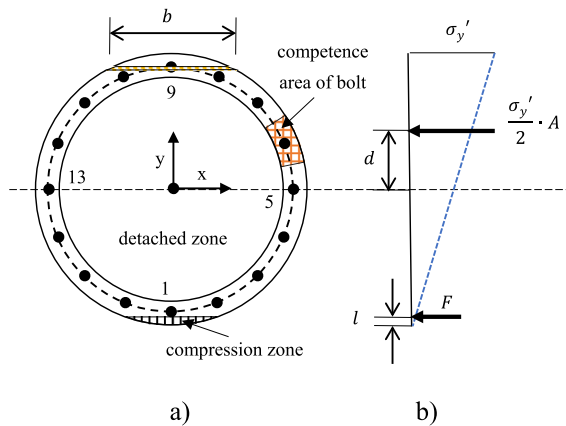
**Fig. 30** The distribution of the deformation and the stress when the bolt began to yield. Where **a** is the cross section of joint, **b** is the stress of the joint

lining deformation and the distribution of the force. The relative rotation deformation of the adjacent segmental lining under the combined application of the buoyancy force and the jack force needs more attention, and the dislocation between the rings is influenced by the gap between the bolt and hole wall. The coordination between the buoyancy force and the jack force and the decrease of gap between the bolt and bolt hole are the way to reduce the relative deformation between the adjacent segments. This paper developed the method to evaluate the joint stiffness and the joint internal force along the longitudinal direction. The exactly evaluation for the strength and the damage risk of joint can and need to be developed furthermore based on the distribution of the internal force.

**Declarations**

**Competing interest**  The authors declare that they have no known competing financial interests or personal relationships that could have appeared to influence the work reported in this paper.

## Appendix A: Derivation of the simplified equation of Joint bending stiffness efficiency (JBSE) based on Boltzmann equation

Because the angle $\varphi$ is difficult to calculate directly based on Eq. 29, finding a simple relationship between JBSE and $\lambda$ is useful for the determination of the longitudinal deformation of the segmental lining. Thanks to the Boltzmann equation (Eq. 54) which can describe a sigmoidal curve, this function is adopted to fitting JBSE varying $\lambda$:

$$y = \frac{A_1 - A_2}{1 + e^{(x-x_0)/dx}} + A_2 \tag{54}$$

where $A_1$ is the initial y value, $A_2$ is the final y value, $x_0$ is the abscissa value of the center point when the ordinate value y is equal to $(A_1 + A_2)/2$, $dx$ is the time constant which can be obtained by the slope at the center point $(x_0, (A_1 + A_2)/2)$, $y' = (A_2 - A_1)/(4 \cdot dx)$.

A modified Boltzmann equation as follows is adopted to better simulate the JBSE-$\lambda$ curve:

$$\text{JBSE}_{Boltz} = \frac{(A_1 - A_2) \cdot \alpha}{1 + e^{(\lambda - \lambda_0)/k}} + A_2 + \Delta \tag{55}$$

where the basic parameters can be obtained from Eqs. 25, 29, 30 and 40: $A_1$ is the bottom limit value which can be obtained when the normal force is equal to 0; $A_2$ is the top limit value which is equal to 1; $\lambda_0$ is the abscissa value when the $JBSE_{Boltz}$ is equal to $(A_1 + A_2)/2$, and can be obtained by an inverse operation based on Eqs. 40, 25 and 29; $k$ is a constant: $k = (A_2 - A_1)/(4 \cdot JBSE')$; where the $JBSE'$ is the slope at the center point $(\lambda_0, (A_1 + A_2)/2)$ and can be obtained by the two points $(\lambda_0 + \Delta\lambda, JBSE_1)$, $(\lambda_0 - \Delta\lambda, JBSE_2)$, where $\Delta\lambda$ is a tiny increment of $\lambda$, $JBSE_1$ and $JBSE_2$ are the corresponding ordinate value;

$\alpha$ is the first modifying parameter for the distance between the bottom limit value and the top limit value, in order to ensure the curve through the two critical points $(0, A_1)$ and $(1, A_2)$. The following equation can be derived and used to calculate this parameter:

$$\alpha = \frac{\left(1 + e^{(1-\lambda_0)/k}\right) \cdot \left(1 + e^{(-\lambda_0)/k}\right)}{e^{(1-\lambda_0)/k} - e^{(-\lambda_0)/k}} \tag{56}$$

$\Delta$ is the second modifying parameter for the top limit value, and is given by:

$$\Delta = -\frac{(A_1 - A_2) \cdot \alpha}{1 + e^{(1-\lambda_0)/k}} \tag{57}$$

According to the case of the Metro tunnel of Ningbo in China, the JBSEs of Eq. 40 are fitted by the Boltzmann function (Boltzman fitting) and the modified Boltzmann equation (Eq. 55) on Fig. 28.

From Fig. 28, it is possible to see how the results of the Boltzmann function and of the modified Boltzmann equation both show a good consistency with the calculated results using Eq. 40. Although the modified Boltzmann equation has a lower R-square value, it has a high precision to describe the JBSE trend varying $\lambda$ parameter.

## Appendix B: Derivation of the limit moment of the second critical point

Based on the analysis of the cases of Sect. 3.2, the height of the compression zone of a shield diameter of 6.2 m is shown in Fig. 29, varying the

bending moment, for different axial forces and bolting systems. From Fig. 29 it is possible to see how the area of the compression zone is very small when the highest bolt in the tensile zone begins to yield.

The bolt tensile stress can be considered approximately as applied on the total joint area. Based on the transformed area method, the stress of the highest point of segmental lining is equal to $\sigma'_y = \sigma_y \cdot n \cdot A_b/A$. The force resultant of the bolt tensile stress is equal to $\sigma'_y \cdot A/2$, and applied on the point which have a distance $d$ from the centroid on the y-axis (Fig. 30). The contact stress of the compression zone is represented by the compressed force $F$ which is applied at a distance $l$ from the lowest point of the section; when the normal force N is equal to 0, the $l$ value is given by the following equation:

$$l = (1 - \sin\varphi) \cdot r + t/2 \tag{58}$$

where the angle $\varphi$ can be obtained by Eq. 27.

Based on the mechanical equilibrium of the normal force and the moment of a joint, the following equations can be obtained:

$$N = F - \frac{\sigma'_y}{2} \cdot A \tag{59}$$

$$M_{lim,2} = F \cdot (R_e - l) + \int_{-R_e}^{R_e} \left(\frac{\sigma'_y}{2R_e} \cdot y\right) \cdot b \cdot y \cdot dy \tag{60}$$

where $F$ is the compressed force of the compression zone; $b$ is the width of the differential element $dy$.

The definition of the moment of inertia $I$ is given by the following equation:

$$\int_{-R_e}^{R_e} b \cdot y^2 \cdot dy = I \tag{61}$$

Substituting Eqs. 59 and 61 into Eq. 60, the limit moment can be finally derived:

$$M_{lim,2} = N \cdot (R_e - l) + \left(R_e - l + \frac{I}{A \cdot R_e}\right) \cdot \frac{\sigma_y}{2} \cdot n \cdot A_b \tag{62}$$

# References

Chaipanna P, Jongpradist P (2019) 3D response analysis of a shield tunnel segmental lining during construction and a parametric study using the ground-spring model. Tunn Undergr Space Technol 90:369–382

Chen RP, Meng FY, Li ZC, Ye YH, Ye JN (2016) Investigation of response of metro tunnels due to adjacent large excavation and protective measures in soft soils. Tunn Undergr Space Technol 58:224–235

Chen RP, Meng FY, Ye YH, Liu Y (2018) Numerical simulation of the uplift behavior of shield tunnel during construction stage. Soils Found 58:370–381

Cheng HZ, Chen RP, Wu HN, Meng FY, Yi YL (2021) General solutions for the longitudinal deformation of shield tunnels with multiple discontinuities in strata. Tunn Undergr Space Technol 107:25

China (2009) Standard for test method of basic properties of construction mortar. China Architecture & Building Press **(in Chinese)**

Einstein HH, Schwartz CW (1979) Simplified analysis for tunnel supports. J Geotech Eng Div 4:499–518

Geng P, Mei SY, Zhang J, Chen PL, Zhang YY, Yan QX (2019) Study on seismic performance of shield tunnels under combined effect of axial force and bending moment in the longitudinal direction. Tunn Undergr Space Technol 91:13

Gil Lorenzo S (2019) Longitudinal beam response of concrete segmental linings simultaneously backfilled with bicomponent grouts. Tunn Undergr Space Technol 90:277–292

Gil Lorenzo S (2021) Structural response of concrete segmental linings in transverse interaction with the TBM. Part 2: Non-axisymmetric conditions. Tunn Undergr Space Technol 116:18

Gong QM, Zhao Y, Zhou JH, Zhou SH (2018) Uplift resistance and progressive failure mechanisms of metro shield tunnel in soft clay. Tunn Undergr Space Technol 82:222–234

Guo XY, Geng P, Wang Q, Chen CJ, Tang R, Yang Q (2021) Full-scale test on seismic performance of circumferential joint of shield-driven tunnel. Soil Dyn Earthq Eng 151:13

Han JY, Zhao W, Jia PJ, Guan YP, Chen Y, Jiang BF (2018) Risk Analysis of the opening of shield-tunnel circumferential joints induced by adjacent deep excavation. J Perform Constr Facil 32:12

Han X, Oreste P, Ye F (2022) The buoyancy of the tunnel segmental lining in the surrounding filling material and its effects on the concrete stress state. Geotech Geol Eng

Huang X, Huang HW, Zhang J (2012) Flattening of jointed shield-driven tunnel induced by longitudinal differential settlements. Tunn Undergr Space Technol 31:20–32

Huang HW, Gong WP, Khoshnevisan S, Juang CH, Zhang DM, Wang L (2015) Simplified procedure for finite element analysis of the longitudinal performance of shield tunnels considering spatial soil variability in longitudinal direction. Comput Geotech 64:132–145

Huang LC, Ma JJ, Lei MF, Liu LH, Lin YX, Zhang ZY (2020) Soil-water inrush induced shield tunnel lining damage and its stabilization: a case study. Tunn Undergr Space Technol 97:16

Koizumi A, Murakami H, Nishino K (1988) Study on the analytical model of shield tunnel in longitudinal direction. J Jpn Soc Civ Eng 394:79–88 (**(in Japanese)**)

Li ZL, Soga K, Wang F, Wright P, Tsuno K (2014) Behaviour of cast-iron tunnel segmental joint from the 3D FE analyses and development of a new bolt-spring model. Tunn Undergr Space Technol 41:176–192

Li XJ, Zhou XZ, Hong BC, Zhu HH (2019) Experimental and analytical study on longitudinal bending behavior of shield tunnel subjected to longitudinal axial forces. Tunn Undergr Space Technol 86:128–137

Liang RZ (2019) Simplified analytical method for evaluating the effects of overcrossing tunnelling on existing shield tunnels using the nonlinear Pasternak foundation model. Soils Found 59:1711–1727

Liang RZ, Xia TD, Huang MS, Lin CG (2017) Simplified analytical method for evaluating the effects of adjacent excavation on shield tunnel considering the shearing effect. Comput Geotech 81:167–187

Liang RZ, Kang C, Xiang LM, Li ZC, Lin CG, Gao K, Guo Y (2021) Responses of in-service shield tunnel to overcrossing tunnelling in soft ground. Environ Earth Sci 80:15

Liao SM, Peng FL, Shen SL (2008) Analysis of shearing effect on tunnel induced by load transfer along longitudinal direction. Tunn Undergr Space Technol 23:421–430

Liu X, Bai Y, Yuan Y, Mang HA (2015) Experimental investigation of the ultimate bearing capacity of continuously jointed segmental tunnel linings. Struct Infrastruct Eng 12:1364–1379

Liu X, Dong ZB, Song W, Bai Y (2018) Investigation of the structural effect induced by stagger joints in segmental tunnel linings: Direct insight from mechanical behaviors of longitudinal and circumferential joints. Tunn Undergr Space Technol 71:271–291

Liu DJ, Wang F, Hu QF, Huang HW, Zuo JP, Tian C, Zhang DM (2020a) Structural responses and treatments of shield tunnel due to leakage: a case study. Tunn Undergr Space Technol 103:18

Liu X, Zhang YM, Bao YH (2020b) Full-scale experimental investigation on stagger effect of segmental tunnel linings. Tunn Undergr Space Technol 102:14

Liu DJ, Tian C, Wang F, Hu QF, Zuo JP (2021) Longitudinal structural deformation mechanism of shield tunnel linings considering shearing dislocation of circumferential joints. Comput Geotech 139:15

Oreste P (2007) A numerical approach to the hyperstatic reaction method for the dimensioning of tunnel supports. Tunn Undergr Space Technol 22:185–205

Oreste P (2013) Face stabilization of deep tunnels using longitudinal fibreglass dowels. Int J Rock Mech Min Sci 58:127–140

Oreste P, Peila D, Marchionni V, Sterling R (2002) Analysis of the problems connected to the sinking of micro-TBMs in difficult grounds. Tunn Undergr Space Technol 13:697

Peila D, Borio L, Pelizza S (2011) The behaviour of a two-componenet back-filling grout used in a tunnel-boring machine. Acta Geotech Slov 8:11

Shi CH, Wang ZX, Gong CJ, Liu JW, Peng Z, Cao CY (2022) Prediction of the additional structural response of segmental tunnel linings induced by asymmetric jack thrusts. Tunn Undergr Space Technol 124:19

Shiba Y, Kawashima K, Obinata N, Kano T (1988) An evaluation method of longitudinal stiffness of shield tunnel

linings for application to seismic response analyses. J Jpn Soc Civ Eng 25:319–327 (**(in Japanese)**)

Shiba Y, Kawashima K, Obinata N, Kano T (1989) Evaluation procedure for seismic stress developed in shield tunnels based on seismic deformation method. J Jpn Soc Civ Eng 25:385–394 (**(in Japanese)**))

Talmon AM, Bezuijen A (2013) Analytical model for the beam action of a tunnel lining during construction. Int J Numer Anal Methods Geomech 37:181–200

Wang Z, Wang LZ, Li LL, Wang JC (2014) Failure mechanism of tunnel lining joints and bolts with uneven longitudinal ground settlement. Tunn Undergr Space Technol 40:300–308

Wu HN, Shen SL, Liao SM, Yin ZY (2015) Longitudinal structural modelling of shield tunnels considering shearing dislocation between segmental rings. Tunn Undergr Space Technol 50:317–323

Wu HN, Shen SL, Yang J, Zhou AN (2018) Soil-tunnel interaction modelling for shield tunnels considering shearing dislocation in longitudinal joints. Tunn Undergr Space Technol 78:168–177

Yan ZG, Peng YC, Ding WQ, Zhu HH, Huang F (2011) Load tests on segment joints of single lining structure of shield tunnel in Qingcaosha Water Conveyance Project. Chin J Geotech Eng 33:1385–1390 (**(in Chinese)**))

Ye F, Gou CF, Sun HD, Liu YP, Xia YX, Zhou Z (2014) Model test study on effective ratio of segment transverse bending rigidity of shield tunnel. Tunn Undergr Space Technol 41:193–205

Yu HT, Cai C, Bobet A, Zhao X, Yuan Y (2019) Analytical solution for longitudinal bending stiffness of shield tunnels. Tunn Undergr Space Technol 83:27–34

Zaheri M, Ranjbarnia M, Dias D, Oreste P (2020) Performance of segmental and shotcrete linings in shallow tunnels crossing a transverse strike-slip faulting. Transp Geotech 23:100333

Zhou SH, Ji C (2014) Tunnel segment uplift model of earth pressure balance shield in soft soils during subway tunnel construction. Int J Rail Transp 2:221–238